



# A critical distance/plane method to estimate finite life of notched components under variable amplitude uniaxial/multi-axial fatigue loading

Luca Susmel<sup>a,\*</sup>, David Taylor<sup>b</sup>

<sup>a</sup> Department of Civil and Structural Engineering, The University of Sheffield, Sheffield S1 3JD, UK

<sup>b</sup> Department of Mechanical Engineering, Trinity College, Dublin 2, Ireland

## ARTICLE INFO

### Article history:

Received 1 July 2011

Received in revised form 1 November 2011

Accepted 6 November 2011

Available online 6 December 2011

### Keywords:

Theory of critical distances

Notch

Critical plane

Variable amplitude loading

## ABSTRACT

The present paper summarises the main features of a design technique we have devised to specifically perform, by post-processing the linear-stress fields in the vicinity of the assumed crack initiation sites, the fatigue assessment of notched components subjected to in-service variable amplitude (VA) uniaxial/multi-axial fatigue loading. In more detail, fatigue damage is estimated through the Modified Wöhler Curve Method (MWCM) applied along with the Theory of Critical Distances (TCDs), the latter being used in the form of the Point Method (PM). According to the philosophy on which the linear-elastic TCD is based, the adopted critical distance is treated as a material property whose length increases as the number of cycles to failure decreases. To correctly apply the MWCM, the orientation of the critical plane is suggested here as being calculated through that direction experiencing the maximum variance of the resolved shear stress. Further, the above direction is used also to perform the cycle counting: since, by definition, the resolved shear stress is a monodimensional stress quantity, fatigue cycles are counted by taking full advantage of the classical three-point Rain Flow method. From a philosophical point of view, the real novelty contained in the present paper is that eventually all the different pieces of theoretical work we have done over the last 15 years by investigating different aspects of the uniaxial/multi-axial fatigue issue are consistently brought together by formalising a design methodology of general validity. The accuracy and reliability of the proposed fatigue assessment technique was checked by using 124 experimental results generated by testing notched cylindrical samples of carbon steel C40. The above tests were run under three different load spectra, by exploring uniaxial as well as in- and out-of-phase biaxial situations, in the latter case the axial and torsional load signals being not only characterised by non-zero mean values, but also by different frequencies. To conclude it can be said that such a systematic validation exercise allowed us to prove that the proposed approach is highly accurate, resulting in estimates falling within the constant amplitude (CA) fully-reversed uniaxial and torsional scatter bands used to calibrate the method itself (this holding true independently of both complexity of the applied VA loading path and sharpness of the tested notch).

© 2011 Elsevier Ltd. All rights reserved.

## 1. Introduction

Examination of the state of the art shows that if, on one hand, several approaches suitable for estimating fatigue lifetime of unnotched engineering materials subjected to VA multi-axial fatigue loading have been formalised and validated through appropriate experimental investigations, on the other hand, only a few attempts have been made so far to devise design methods specifically devoted to the fatigue assessment of notched components damaged by in-service VA multi-axial loading paths.

In more detail, with regard to the problem of estimating VA medium/high-cycle fatigue damage in unnotched materials, so far the scientific community has focussed its attention mainly on

the formalisation of approaches taking full advantage of the critical plane concept, such a classical idea being applied in terms of either stress or energy quantities [1–5]. On the contrary, to estimate VA fatigue lifetime of unnotched components failing in the low/medium-cycle fatigue regime, a lot of work has been done by several researchers [6–12] to check the accuracy and reliability of both the SWT parameter [13,14], Kandil, Brown and Miller's criterion [15,16], and Fatemi and Socie's method [17,18].

As to the design strategies that have been explored so far, it is worth mentioning here also that the above criteria were attempted to be applied by post-processing the input load histories not only in the time, but also in the frequency domain [19–22].

Turning back to the problem of estimating fatigue lifetime of notched components damaged by in-service VA multi-axial loading paths, it can be highlighted here that the research work done so far has been mainly based on the idea of extending the use of the

\* Corresponding author.

E-mail address: [l.susmel@sheffield.ac.uk](mailto:l.susmel@sheffield.ac.uk) (L. Susmel).

classical strain-based critical plane approaches mentioned above also to those VA situations involving stress/strain concentration phenomena [23,24]. As to the in-field usage of such a strategy, it has to be said that, unfortunately, correctly estimating root stresses and strains by simultaneously modelling the material elasto-plastic stabilised response under VA loading is never a simple task: this should make it evident that properly using the above approaches results in an inevitable increase of the time and costs of the design process.

In this complex scenario, the present paper attempts to formalise a novel design methodology based on the use of the MWCM [25] (applied in conjunction with the TCD [26]) suitable for estimating fatigue lifetime under VA uniaxial/multiaxial fatigue loading by directly post-processing the linear-elastic stress fields damaging the material in the vicinity of the stress raisers being assessed.

## 2. The MWCM applied along with the PM

The MWCM [25,27] is a bi-parametrical critical plane approach which postulates that lifetime under CA multiaxial fatigue loading can directly be estimated through the shear stress amplitude, the mean normal stress,  $\sigma_{n,m}$ , and the amplitude of the normal stress,  $\sigma_{n,a}$ , relative to that plane (i.e., the so-called critical plane) experiencing the maximum shear stress amplitude,  $\tau_a$  [28,29]. In order to simultaneously take into account the above stress components, their combined effect is directly evaluated by means of the following stress ratio [30]:

$$\rho_{\text{eff}} = \frac{m \cdot \sigma_{n,m} + \sigma_{n,a}}{\tau_a}, \quad (1)$$

where mean stress sensitivity index  $m$  is a material property to be determined experimentally and varying in the range 0–1 [25,30]. Thanks to the way  $\rho_{\text{eff}}$  is defined, such a stress ratio is seen to be sensitive not only to the presence of superimposed static stresses, but also to the degree of multiaxiality and non-proportionality of the applied loading path [25]. As to the latter aspect, it is worth recalling here that in unnotched materials a fully-reversed uniaxial loading results in a  $\rho_{\text{eff}}$  ratio invariably equal to unity, whereas under fully-reversed torsional loading  $\rho_{\text{eff}}$  equals zero [25].

The way the MWCM works in practise is schematically shown by the modified Wöhler diagram [27] reported in Fig. 1a, such a log–log chart plotting the shear stress amplitude relative to the critical plane,  $\tau_a$ , against the number of cycles to failure,  $N_f$ . According to the experimental evidence, it is seen that [25,31,32], given the material, different fatigue curves are obtained as ratio  $\rho_{\text{eff}}$  varies (Fig. 1a). If the classical schematisation used to summarise fatigue results is adopted also when they are plotted in Modified Wöhler diagrams, any Modified Wöhler curve can unambiguously be defined through the following linear relationships [25,31,32]:

$$k_{\tau}(\rho_{\text{eff}}) = (k - k_0) \cdot \rho_{\text{eff}} + k_0 \quad \text{for } \rho_{\text{eff}} \leq \rho_{\text{lim}} \quad (2)$$

$$k_{\tau}(\rho_{\text{eff}}) = k_{\tau}(\rho_{\text{lim}}) = (k - k_0) \cdot \rho_{\text{lim}} + k_0 \quad \text{for } \rho_{\text{eff}} > \rho_{\text{lim}} \quad (3)$$

$$\tau_{A,\text{Ref}}(\rho_{\text{eff}}) = \left( \frac{\sigma_A}{2} - \tau_A \right) \cdot \rho_{\text{eff}} + \tau_A \quad \text{for } \rho_{\text{eff}} \leq \rho_{\text{lim}} \quad (4)$$

$$\tau_{A,\text{Ref}}(\rho_{\text{eff}}) = \tau_{A,\text{Ref}}(\rho_{\text{lim}}) = \left( \frac{\sigma_A}{2} - \tau_A \right) \cdot \rho_{\text{lim}} + \tau_A, \quad \text{for } \rho_{\text{eff}} > \rho_{\text{lim}} \quad (5)$$

where

$$\rho_{\text{lim}} = \frac{\tau_A}{2\tau_A - \sigma_A}. \quad (6)$$

In more detail, given a modified Wöhler curve characterised by a certain value of  $\rho_{\text{eff}}$ ,  $k_{\tau}(\rho_{\text{eff}})$  is its negative inverse slope and

$\tau_{\text{Ref}}(\rho_{\text{eff}})$  is its reference shear stress amplitude extrapolated at  $N_A$  cycles to failure (Fig. 1a). Further, as explained in Fig. 1a,  $k$  is the negative inverse slope and  $\sigma_A$  the endurance limit at  $N_A$  cycles to failure characterising the fully-reversed uniaxial fatigue curve ( $\rho_{\text{eff}} = 1$ ), whereas  $k_0$  and  $\tau_A$  are the corresponding quantities describing the fully-reversed torsional fatigue curve ( $\rho_{\text{eff}} = 0$ ).

It is worth observing here also that both the negative inverse slope and the reference shear stress amplitude defining the fatigue curves to be used to estimate fatigue damage under a  $\rho_{\text{eff}}$  ratio larger than limit value  $\rho_{\text{lim}}$ , Eq. (6), are assumed to be constant and equal to  $k_{\tau}(\rho_{\text{lim}})$  and to  $\tau_{\text{Ref}}(\rho_{\text{lim}})$ , respectively – see Eqs. (3) and (5) [25,30,33]. This correction, which plays a role of primary importance in the overall accuracy of the MWCM, was introduced in light of the experimental evidence that, given the shear stress amplitude relative to the propagation plane, when micro/meso cracks are fully open, an increase of the normal mean stress does not result in any further increase of fatigue damage [34].

To conclude it can be observed that, according to the schematic modified Wöhler diagram sketched in Fig. 1a, given the  $\rho_{\text{eff}}$  ratio as well as the shear stress amplitude,  $\tau_a$ , relative to the critical plane, the corresponding number of cycles to failure can directly be predicted according to the following trivial relationship [25]:

$$N_{f,e} = N_A \cdot \left[ \frac{\tau_{A,\text{ref}}(\rho_{\text{eff}})}{\tau_a} \right]^{k_{\tau}(\rho_{\text{eff}})}, \quad (7)$$

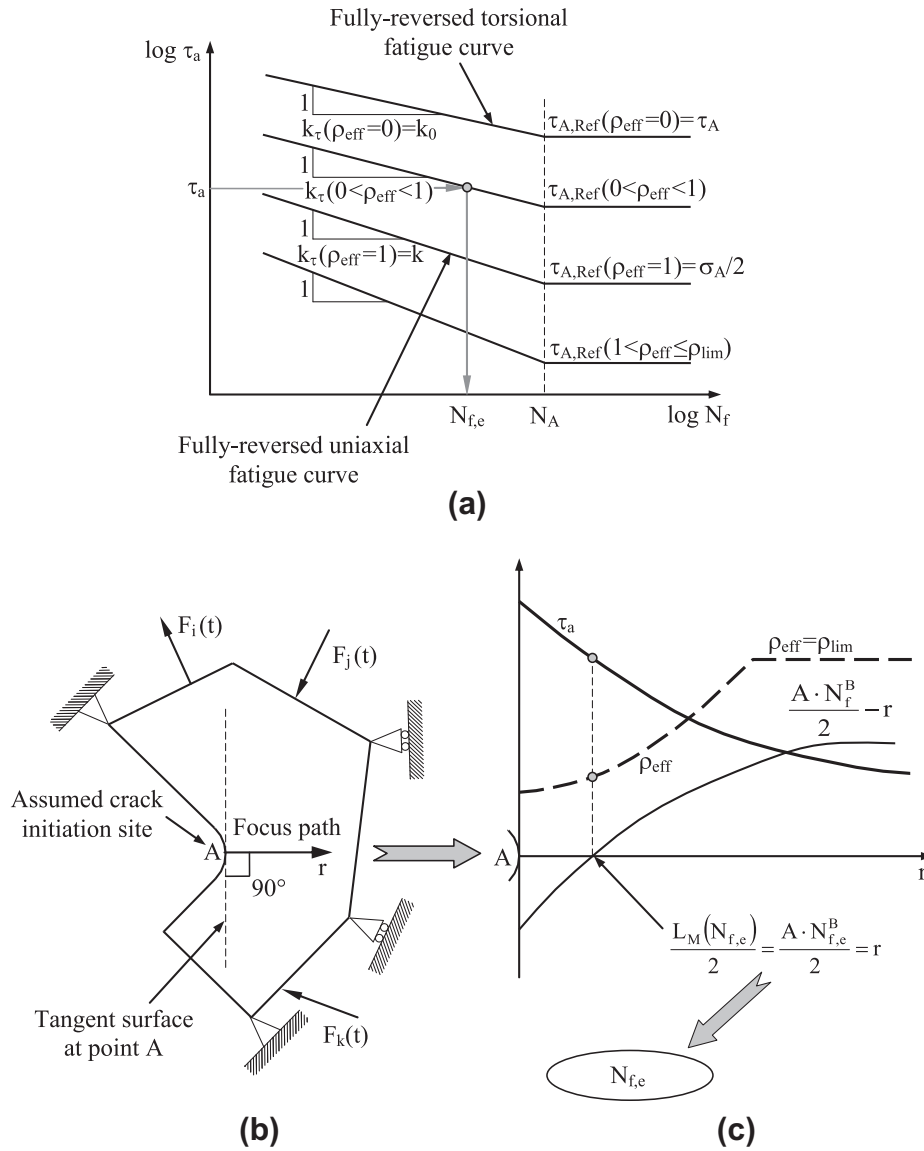
the appropriate modified Wöhler curve being obviously defined through Eqs. (2)–(6).

Thanks to its specific features, the MWCM can be used to predict fatigue damage not only in unnotched materials [31,32], but also in notched components, where in the latter case it can be applied in terms of both nominal [25,27] and local stresses [35–39]. In more detail, our multiaxial fatigue criterion can be used in conjunction with the TCD, formalised in the form of the PM, to estimate finite lifetime of notched components subjected to CA uniaxial/multiaxial fatigue loading [39], the correct way of employing our criterion for such a purpose being explained in Fig. 1b and c. As to the PM's *modus operandi*, it is worth recalling here that it was first proposed by Peterson [40], who argued that high-cycle fatigue strength of notched components could accurately be estimated by directly post-processing the stress state at a given distance from the assumed crack initiation point, such a distance being treated as a material property.

Before briefly reviewing the in-field usage of such a method, it is worth recalling here that the critical distance to be used to estimate finite life of notched components is suggested as being defined as follows [25,38,39]:

$$L_M(N_f) = A \cdot N_f^B, \quad (8)$$

where  $A$  and  $B$  are material fatigue constants to be estimated from the fully-reversed unnotched fatigue curve as well as from a fully-reversed notch fatigue curve generated by testing samples containing a known geometrical feature [38,41]. With regard to the critical distance value to be used to estimate finite lifetime, it is worth observing here that, according to definition (8), as the number of cycles to failure decreases, length  $L_M$  increases. This assumption takes as a starting point the experimental evidence that the size of the plastic zone at the notch tip varies as the magnitude of the applied cyclic force changes: accordingly, since the PM as employed in the present study is applied by forcing engineering materials to obey a linear-elastic constitutive law, the cyclic plastic behaviour of ductile metals is accommodated into a linear-elastic model by simply making the size of the process zone (which is assumed to be related to  $L_M$  [25,26]) increase as the amplitude of the applied cyclic stress increases. The above considerations should make it evident that such an idea is, by nature, suitable for designing engineering mate-



**Fig. 1.** Modified Wöhler diagram (a) and in-field usage of the MWCM applied along with the PM to estimate lifetime of notched components subjected to CA uniaxial/multiaxial fatigue loading (b, c).

rials failing solely in the medium/high-cycle fatigue regime, that is, for  $N_f$  values larger than about  $10^3$  cycles to failure.

Turning back to the proper way of performing the fatigue assessment according to our local approach, initially the linear-elastic stress field along the focus path has to be calculated by taking full advantage of either analytical or numerical tools, where the focus path is a straight line emanating from the assumed crack initiation location and perpendicular to the component surface at the hot spot itself (Fig. 1b) [25]. It is worth remembering here also that the focus path is suggested as being taken coincident with the notch bisector when stress concentrators are modelled by imposing that the notch root radius equals zero [25]. As soon as the focus path is defined, both maximum shear stress amplitude  $\tau_a$  and ratio  $\rho_{eff}$  have to be calculated along the focus path itself, by plotting, as shown in Fig. 1c, such stress quantities against distance  $r$ . From the calculated values for both  $\tau_a$  and  $\rho_{eff}$ , the corresponding Modified Wöhler curve can then be determined, through Eqs. (2)–(6), at any distance  $r$  from the notch tip, by subsequently estimating the resulting number of cycles to failure,  $N_{f,e}$  – Eq. (7). After estimating  $N_{f,e}$  along the focus path, the notched component being assessed is

assumed to fail at the number of cycles to failure as given by the following condition (Fig. 1c) [40]:

$$\frac{L_M(N_{f,e})}{2} - r = 0 \Rightarrow \frac{A \cdot N_{f,e}^B}{2} - r = 0. \tag{9}$$

To conclude, it is important to remember here that the constants in the  $L_M$  vs.  $N_f$  relationship, Eq. (8), used to estimate lifetime according to condition (9) have to be determined by always employing fatigue results generated under fully-reversed loading, since, thanks to the sensitivity of ratio  $\rho_{eff}$  to the presence of superimposed static loadings, the detrimental effect of non-zero mean stresses is directly taken into account by the MWCM itself [25,39].

### 3. Stress quantities relative to the critical plane under VA fatigue loading

As briefly mentioned at the beginning of the previous section, the MWCM is based on the assumption that the plane of maximum shear stress amplitude is also the one on which fatigue damage

reaches its maximum value. Taking as a starting point the above definition, the hypothesis can be formed that the critical plane under VA fatigue loading coincides with that material plane containing the direction which experiences the maximum variance of the resolved shear stress [42–44]. As to the above assumption, it can be remembered here that, by definition, the variance of a signal quantifies the amount of variation of the signal itself within the two extremes delimiting the maximum range, the variance being independent from the mean value of the considered signal. Accordingly, as far as time-variable stress components are concerned, the variance of a stress signal can be assumed as being proportional to the associated fatigue damage extent [42,45].

Since the in-field procedure suitable for determining the critical plane according to the above strategy has already been discussed in great detail elsewhere [44,46], by also investigating the numerical aspects of the necessary optimisation procedure [47], only the fundamental ingredients of the so-called Maximum Variance Method (MVM) [42,44] will briefly be recalled in what follows.

Consider then a generic point, O, belonging to a body subjected to a complex system of time-variable forces (Fig. 2a), the investigated load history being defined in the time interval  $[0, T]$ . According to the MVM, the critical plane is the one containing that direction, MV, experiencing the maximum variance of resolved shear stress  $\tau_{MV}(t)$  (Fig. 2b) [46,47]. In light of the obvious fact that  $\tau_{MV}(t)$  is a monodimensional stress quantity defined in the time interval  $[0, T]$ , its mean value is equal to:

$$\bar{\tau}_m = \frac{1}{T} \int_0^T \tau_{MV}(t) \cdot dt, \quad (10)$$

whereas its equivalent amplitude can be calculated as [46,47]:

$$\bar{\tau}_a = \sqrt{2 \cdot \text{Var}[\tau_{MV}(t)]}, \quad (11)$$

$\text{Var}[\tau_{MV}(t)]$  being the variance of the shear stress resolved along direction MV, i.e.:

$$\text{Var}[\tau_{MV}(t)] = \frac{1}{T} \int_0^T [\tau_{MV}(t) - \bar{\tau}_m]^2 \cdot dt \quad (12)$$

Similarly, the amplitude of the stress perpendicular to the critical plane ( $\sigma_n(t)$  in Fig. 2b) takes on the following value:

$$\bar{\sigma}_{n,a} = \sqrt{2 \cdot \text{Var}[\sigma_n(t)]} \quad (13)$$

where

$$\text{Var}[\sigma_n(t)] = \frac{1}{T} \int_0^T [\sigma_n(t) - \bar{\sigma}_{n,m}]^2 \cdot dt \quad (14)$$

$$\bar{\sigma}_{n,m} = \frac{1}{T} \int_0^T \sigma_n(t) \cdot dt. \quad (15)$$

The schematic charts sketched in Fig. 2c and d graphically summarise the meaning of definitions (11) and (13) [46]: the equivalent amplitude of both resolved shear stress  $\tau_{MV}(t)$  and normal stress  $\sigma_n(t)$  is proportional to the amount of variation of the stress signals themselves.

Turning back to the MWCM, as mentioned in the previous section, it postulates that, under CA loading, the degree of multiaxiality and non-proportionality of the stress state at the assumed critical point has to be directly evaluated through ratio  $\rho_{\text{eff}}$ , such a stress ratio being sensitive also to the presence of superimposed static stresses. By taking full advantage of identity (1), in the presence of VA fatigue loading such a stress ratio can directly be re-defined as follows [46]:

$$\bar{\rho}_{\text{eff}} = \frac{m \cdot \bar{\sigma}_{n,m} + \bar{\sigma}_{n,a}}{\bar{\tau}_a} \quad (16)$$

It is worth concluding the present section by observing that, since the MWCM treats the mean stress sensitivity as a material property, the  $m$  value to be used in identity (16) to quantify the

damaging effect of the mean stress perpendicular to the critical plane can directly be estimated from a CA uniaxial fatigue curve generated under a load ratio,  $R = \sigma_{\text{min}}/\sigma_{\text{max}}$ , larger than  $-1$  [25,30].

#### 4. Estimating fatigue lifetime of notched components under VA fatigue loading

In order to formalise our novel VA multiaxial fatigue lifetime estimation technique, consider the notched component sketched in Fig. 2a. Such a component is assumed to be subjected to a complex system of time-variable forces resulting in a time-variable multiaxial stress field acting on the material in the vicinity of the stress raiser being assessed. After defining the focus path according to the geometrical rule briefly recalled in Section 2, consider the stress state at a given point, O, positioned, along the focus path itself, at a distance from the assumed crack initiation site equal to  $r$  (Fig. 2a). From the stress state at point O the orientation of the critical plane can directly be determined by taking full advantage of the MVM (Fig. 2b) [46,47]. As soon as direction MV is known, the equivalent amplitude (Fig. 2c) of both resolved shear stress  $\tau_{MV}(t)$  and normal stress  $\sigma_n(t)$  have to be calculated according to definitions (11) and (13), respectively, by subsequently determining the resulting critical plane stress ratio,  $\bar{\rho}_{\text{eff}}$  – see Eq. (16). To evaluate the fatigue damage associated with the investigated VA load history, the constants of the appropriate modified Wöhler curve can now be estimated from the MWCM's governing equations (Figs 2d and e), where, to properly handle VA load histories,  $\rho_{\text{eff}}$  has to be replaced in Eqs. (2)–(5) with  $\bar{\rho}_{\text{eff}}$ . Further, in order to correctly take into account the damaging effect of those cycles of low shear stress amplitude, as recommended by Haibach [48], the negative inverse slope in the long-life regime is suggested as being corrected as follows [46] (Fig. 2e):

$$m_\tau(\bar{\rho}_{\text{eff}}) = 2 \cdot k_\tau(\bar{\rho}_{\text{eff}}) - 1 \quad \text{for } \bar{\rho}_{\text{eff}} \leq \rho_{\text{lim}} \quad (17)$$

$$m_\tau(\bar{\rho}_{\text{eff}}) = 2 \cdot k_\tau(\rho_{\text{lim}}) - 1 = \text{const} \quad \text{for } \bar{\rho}_{\text{eff}} > \rho_{\text{lim}} \quad (18)$$

where whenever it is not known from the experiments, the position of the knee point ( $N_{\text{kp}}$  in Fig. 2e) can be estimated by taking full advantage of the available recommendations [49].

After defining the pertinent modified Wöhler curve, the shear stress resolved along direction MV,  $\tau_{MV}(t)$ , has to be post-processed in order to perform the cycle counting. In particular, since  $\tau_{MV}(t)$  is a monodimensional stress quantity, the corresponding load spectrum (Fig. 2g) can directly be built by counting the shear stress cycles through the classical three-point Rain Flow method [46,50] (Fig. 2f). Subsequently, by taking full advantage of the determined resolved shear stress spectrum, the fatigue damage content associated with any counted cycle can be estimated through the appropriate modified Wöhler curve as follows:

$$D_i = \frac{n_i}{N_{f,i}} \quad \text{for } i = 1, 2, \dots, j \quad (19)$$

the resulting damage content of the investigated load history being equal to (Fig. 2h):

$$D_{\text{tot}} = \sum_{i=1}^j D_i = \sum_{i=1}^j \frac{n_i}{N_{f,i}} \quad (20)$$

The total damage content determined as above has to be used now to calculate an equivalent number of cycles to failure,  $N_{f,\text{eq}}$ , suitable for estimating, through the  $L_M$  vs.  $N_f$  relationship, the critical distance value. In particular,  $N_{f,\text{eq}}$  can be determined by considering an equivalent load history whose damage content assures the following condition:

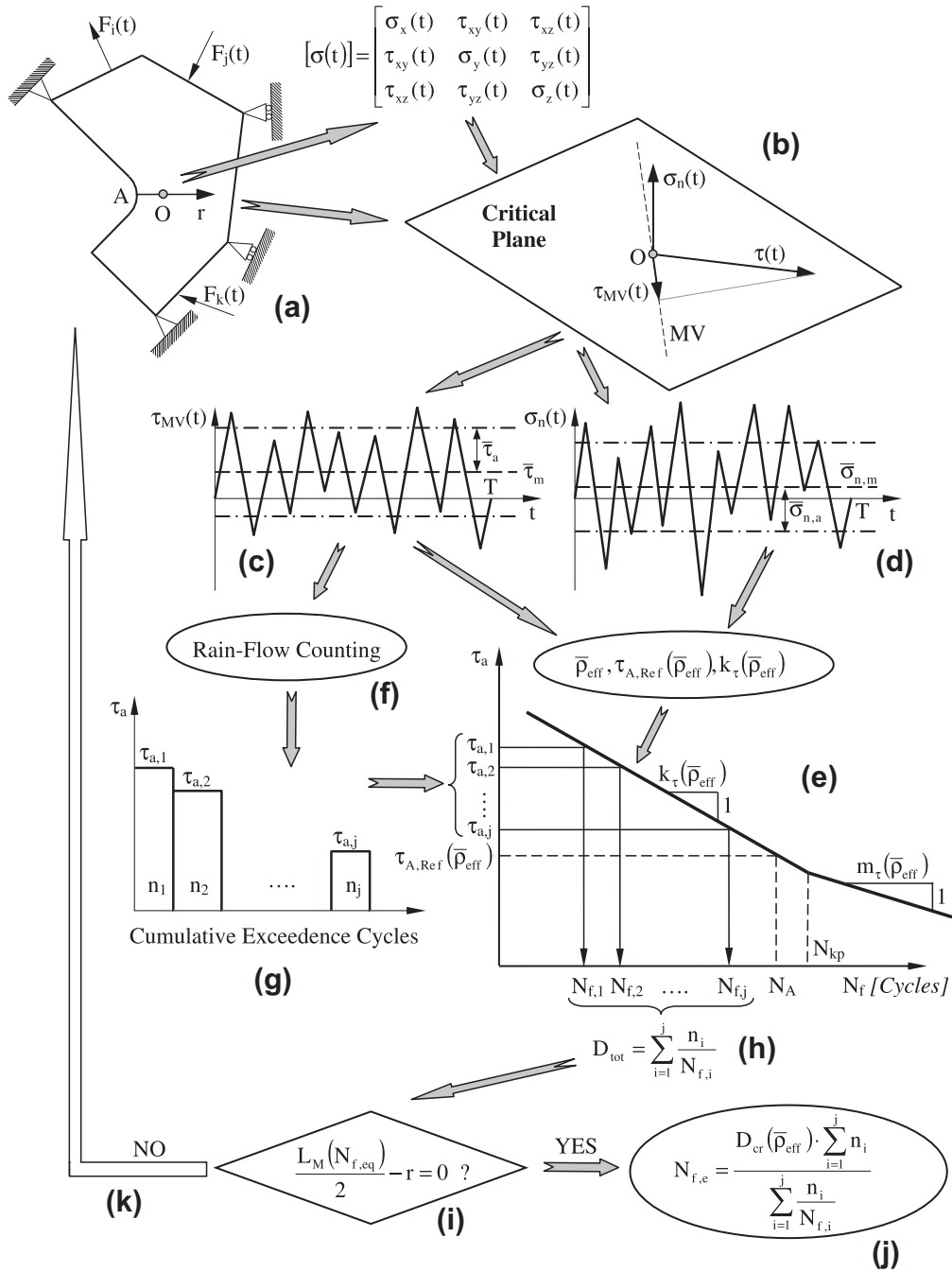


Fig. 2. In-field use of the proposed VA design methodology.

$$\frac{n_{eq}}{N_{f,eq}} = \sum_{i=1}^j \frac{n_i}{N_{f,i}} = D_{tot} \quad (21)$$

If the equivalent number of cycles,  $n_{eq}$ , is taken equal to the sequence length,  $n_{tot}$ , of the investigated load history,  $N_{f,eq}$  can directly be calculated as:

$$N_{f,eq} = \frac{n_{tot}}{D_{tot}} = \frac{\sum_{i=1}^j n_i}{\sum_{i=1}^j \frac{n_i}{N_{f,i}}} \quad (22)$$

With regard to the validity of identity (22), it is worth remembering here that the same assumption leads to the following well-known equivalent uniaxial stress amplitude which is widely used in situations of practical interest [51], being also recommended by several design codes [52,53]:

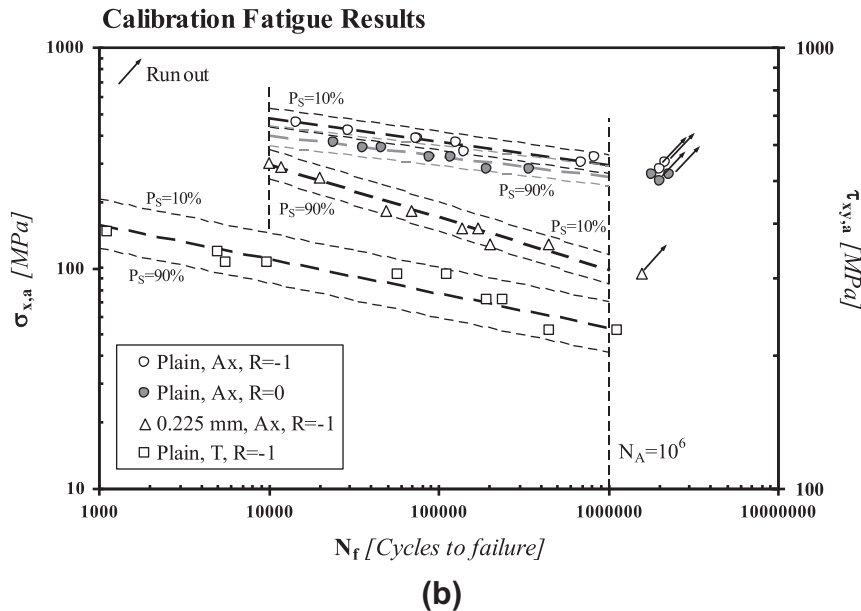
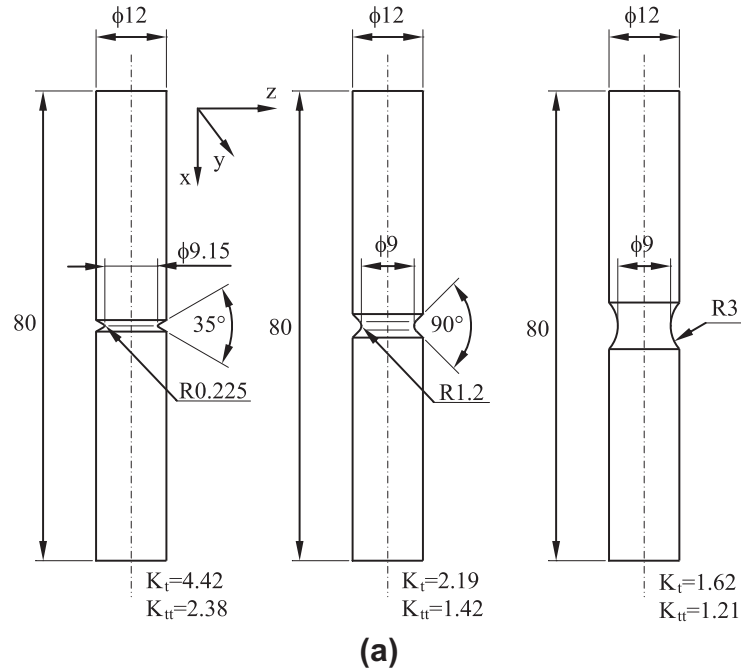
$$\sigma_{a,eq} = \sqrt{\frac{\sum_{i=1}^j n_i \cdot \sigma_a^k}{n_{tot}}}$$

According to the reasoning summarised above, the  $L_M$  vs.  $N_f$  relationship, Eq. (8), can then be rewritten to efficiently handle VA fatigue situations as:

$$L_M(N_f) = A \cdot N_{f,eq}^B = A \cdot \left( \frac{\sum_{i=1}^j n_i}{\sum_{i=1}^j \frac{n_i}{N_{f,i}}} \right)^B, \quad (23)$$

where fatigue constants  $A$  and  $B$  are those estimated for the material being assessed by following the standard procedure which is based on the use of both the CA fully-reversed unnotched uniaxial fatigue curve and a CA fully-reversed notch fatigue curve





**Fig. 3.** Geometries of the tested notched samples (dimensions in millimetres) (a) and fatigue results used to calibrate the constants both in the MWCM's governing equations and in the  $L_M$  vs.  $N_f$  relationship (Ax = axial loading, T = torsional loading, R = load ratio) (b).

determined by testing samples containing a known geometrical feature [39,41]. If the critical distance value calculated according to Eq. (22) assures the following condition (Fig. 2j):

$$\frac{L_M(N_{f,eq})}{2} - r = 0 \Rightarrow \frac{A \cdot N_{f,eq}^B}{2} - r = 0. \quad (24)$$

then the total number of cycles to failure can be estimated as follows (Fig. 2j):

$$N_{f,e} = \frac{D_{cr}(\bar{\rho}_{eff}) \cdot n_{tot}}{D_{tot}} = \frac{D_{cr}(\bar{\rho}_{eff}) \cdot \sum_{i=1}^j n_i}{\sum_{i=1}^j \frac{n_i}{N_{f,i}}} \quad (25)$$

where  $D_{cr}(\bar{\rho}_{eff})$  is the critical value of the damage sum. As to  $D_{cr}(\bar{\rho}_{eff})$ , such a quantity is suggested here as being defined as [46]:

$$D_{cr}(\bar{\rho}_{eff}) = d_1 \cdot \bar{\rho}_{eff} + d_2, \quad \text{for } \bar{\rho}_{eff} \leq \rho_{lim} \quad (26)$$

$$D_{cr}(\rho_{lim}) = d_1 \cdot \rho_{lim} + d_2, \quad \text{for } \bar{\rho}_{eff} > \rho_{lim} \quad (27)$$

$d_1$  and  $d_2$  being two fatigue constants to be determined by running appropriate experiments.

On the contrary, if condition (24) is not assured, it is evident that the same procedure as the one summarised above has to be re-applied by changing the distance, along the focus path, of the reference point, O, used to estimate  $N_{f,e}$ . Such a procedure has to be reiterated until convergence has occurred (Fig. 2k).

Turning back to identity (26), it is worth observing here that  $D_{cr}(\bar{\rho}_{eff})$  is defined by assuming that the critical value of the damage sum may vary as the degree of multiaxiality and non-proportionality, measured through ratio  $\bar{\rho}_{eff}$ , of the stress state at the investigated material point changes. As to the recommended

values for  $D_{cr}(\bar{\rho}_{eff})$ , initially it has to be remembered here that, in real mechanical components subjected to VA uniaxial fatigue loading, the experimental value of the damage sum is seen to vary in the range 0.02–5, the average value being equal to 0.27 for steel and to 0.37 for aluminium [51]. Further, in the most general case, the critical value of the damage sum depends also on the complexity of the assessed VA stress state. As to the latter aspect, an interesting example is represented by steel weldments. In more detail, by performing an accurate experimental investigation Sonsino and Kueppers [54] observed that, for their tube-to-plate welded joints tested under Gaussian Spectra with sequence length of  $5 \times 10^4$  cycles, the critical value of the damage sum was equal to 0.08 under VA pure bending, to 0.38 under VA pure torsion and to 0.35 under in-phase and  $90^\circ$  out-of-phase VA combined bending and torsion. Therefore, according to the above experimental evidence which applies also to non-welded metallic components [46], the method formalised in the present paper is based on the assumption that the critical value of the damage sum can vary as the degree of multi-axiality and non-proportionality of the critical stress state changes, such an hypothesis being formalised by imposing a linear relationship between  $D_{cr}$  and  $\bar{\rho}_{eff}$  [46].

To conclude, it is worth observing that when the method discussed in the present section is used to design notched components against CA uniaxial/multi-axial fatigue loading, the estimated number of cycles of failure is exactly the same as the one which would be predicted by using the approach we have specifically formalised to deal with CA loading paths (Fig. 1b): this important aspect should make it evident that there exists a sound consistency between the idea formalised in the present paper and suitable for designing notched components against VA fatigue loading and the approach we have devised by considering solely CA situations [39].

## 5. Experimental details and results

In order to check the accuracy and reliability of the fatigue design method formalised in the previous section, a systematic experimental investigation was carried out by testing the V-notched cylindrical samples sketched in Fig. 3a, the above figure reporting also the values of the net stress concentration factors calculated, through refined finite element (FE) models, under both tension,  $K_t$ , and torsion,  $K_{tt}$ .

The investigated material was medium-carbon steel C40 that had an ultimate tensile stress equal to 852 MPa, a yield stress of 672 MPa, and a Young's modulus of 209,000 MPa.

The fatigue properties of the parent material were determined by testing, at a frequency of 4 Hz, unnotched cylindrical samples under both fully-reversed axial loading, zero-tension, and fully-reversed torsion. The above fatigue results are summarised in the Wöhler diagram reported in Fig. 3b, such a chart displaying, in terms of nominal net stress amplitude, also the experimental data generated by testing, under CA fully-reversed axial loading, the V-notched samples with root radius,  $r_n$ , equal to 0.225 mm. As to the performed statistical reanalysis, it is worth observing here that the scatter bands plotted in the chart of Fig. 3b were calculated under the hypothesis of a log-normal distribution of the number of cycles to failure for each stress level and assuming a confidence level equal to 95% [55]. The corresponding fatigue curves, estimated for a probability of survival,  $P_S$ , equal to 50%, are summarised in Table 1 in terms of negative inverse slope,  $k$  and  $k_0$ , endurance limit,  $\sigma_A$  and  $\tau_A$ , and scatter ratio of the stress amplitude,  $T_\sigma$  and  $T_\tau$ , at  $N_A$  cycles to failure for 90% and 10% probabilities of survival. According to the fatigue behaviour displayed by the parent material under axial loading (see the chart of Fig. 3b), the reference number of cycles to failure,  $N_A$ , was taken equal to  $10^6$ .

The chart reported in Fig. 4a shows the profiles of the three investigated load spectra, where axial nominal net stress  $\Sigma_{a,i}$  and torsional nominal net stress  $T_{a,i}$  denote the amplitude of the  $i$ -th cycle, whereas  $\Sigma_{a,max}$  and  $T_{a,max}$  denote the maximum values in the spectrum of the above nominal stress amplitudes. Spectrum 1000RA, having sequence length,  $n_{tot}$ , equal to 1000 cycles, was derived from the classical Rayleigh distribution, whereas spectrum 2500L ( $n_{tot} = 250$  cycles) was adopted to investigate the accuracy of our method in estimating fatigue lifetime under nominal uniaxial fatigue loading in the presence of overloadings. Finally, spectrum 50BSP ( $n_{tot} = 50$  cycles) was designed to investigate, according to the characteristics of our biaxial testing machine, the fatigue behaviour of the considered V-notched cylindrical samples under complex VA biaxial load histories. Spectra 1000RA and 2500L were used to investigate the notch fatigue behaviour of the tested carbon steel solely under VA nominal uniaxial fatigue loading, the sinusoidal cycles being applied in random order with a frequency of 4 Hz. On the contrary, due to the intrinsic limits of our biaxial testing machine in terms of number of turning points, spectrum 50BSP was applied by adopting a triangular shape for the wave form. For the sake of completeness, Fig. 4b schematically shows the nominal loading paths, plotted considering one single cycle, which were investigated to generate the notch results not only under uniaxial, but also under biaxial nominal loading, where: Ax = axial loading, T = torsion, Bi = biaxial loading, ZMS = zero mean stress, N-ZMS = non-zero mean stress, IPh = in-phase loading, OoPH = out-of-phase loading, and, finally, F is the ratio between the frequencies of the applied axial and torsional nominal loading.

All the generated results are summarised in Tables 2–4, where the performed tests are described in terms of adopted spectrum, maximum amplitude in the spectrum of the axial,  $\Sigma_{a,max}$ , and torsional,  $T_{a,max}$ , nominal net stress, axial,  $\Sigma_m$ , and torsional,  $T_m$ , mean nominal net stress, out-of-phase angle,  $\delta$ , ratio  $F$  between the frequencies of the two loading channels, and, finally, experimental value of the number of cycles to failure,  $N_f$ . It is worth observing here that, to check the accuracy of the proposed approach, fatigue failures were defined by 50% axial stiffness drop calculated under the maximum amplitude applied in the spectrum. To investigate the cracking behaviour of the notched samples instead, any tests were run up to the complete breakage of the specimens themselves.

As to the results listed in the above tables, it is worth observing here that, since all the cycles were applied in random order, the instantaneous values of the load channels were gathered during testing systematically, by subsequently post-processing the recorded signals to verify *a posteriori* the correspondence between theoretical and applied load spectrum, the cycle counting being performed according to the three-point Rain-Flow method [50]. Another important experimental aspect which deserves to be mentioned explicitly is that, since, as said above, the cycles were applied in random order also under VA biaxial loading, the ratio between the amplitudes of the axial and torsion nominal stress was different from cycle to cycle during testing. To conclude, it can be pointed out that the experimental values of the number of cycles to failure listed in Tables 2–4 and obtained under VA biaxial loading at different frequencies were counted through the signals gathered from the torsional actuator.

## 6. Observed cracking behaviour under VA biaxial loading

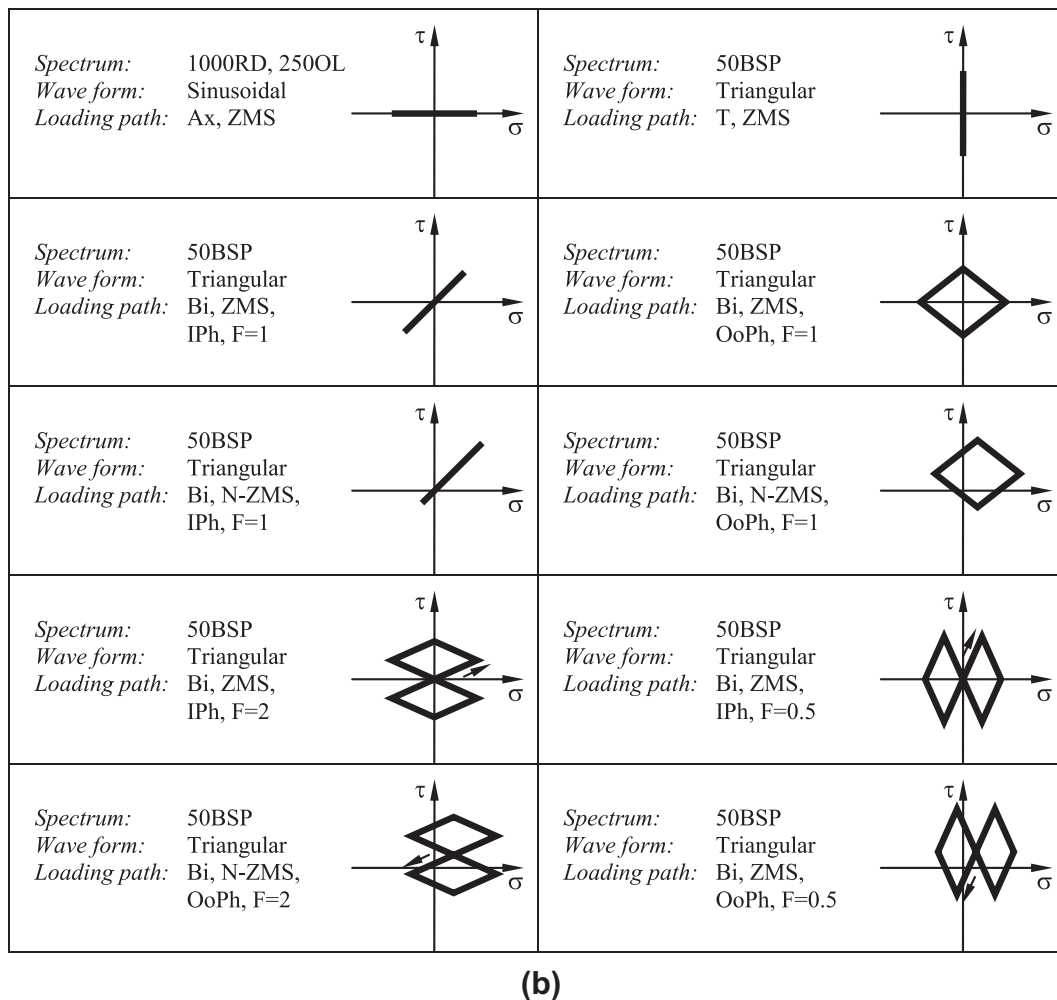
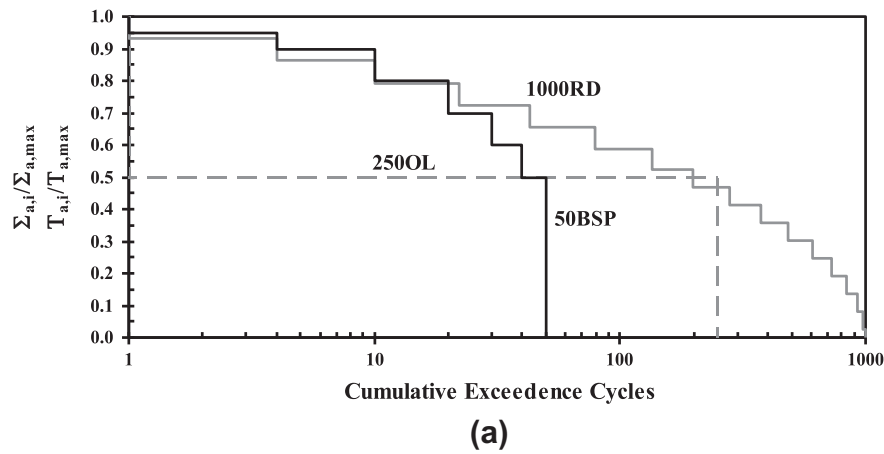
Before systematically checking the accuracy of the proposed VA fatigue design method through the generated experimental results, the fracture surfaces of the tested specimens were investigated in depth in order to qualitatively single out the predominant cracking

**Table 1**  
Summary of the experimental fatigue results generated under CA axial loading as well as under CA torsion.

Specimen type	N. of data	$r_n$ (mm)	$d_g$ (mm)	$d_n$ (mm)	$\omega$ (°)	$R$	$k(k_0)$	$\sigma_A^a$ (MPa)	$\tau_A^a$ (MPa)	$T_\sigma$	$T_\tau$	$K_t$	$K_{tt}$
Plain	10	–	12	6	–	–1	9.4	292.8	–	1.211	–	1.06	1.02
	10	–	12	6	–	0	10.8	260.0	–	1.236	–	–	–
	10	–	12	11	–	–1	12.8	–	231.7	–	1.297	–	–
Sharp	10	0.225	12	9.15	35	–1	4.2	97.8 <sup>b</sup>	–	1.361	–	4.42	2.38

<sup>a</sup> Reference stress amplitude extrapolated at  $10^6$  cycles to failure.

<sup>b</sup> Nominal net stress.



**Fig. 4.** Adopted load spectra (a) and investigated loading paths (one single cycle is plotted for each loading configuration) (b).



**Table 2**

Summary of the experimental results generated by testing the notched specimens with root radius equal to 0.225 mm under VA fatigue loading.

Code	Spectrum	$\Sigma_{a,max}$ (MPa)	$\Sigma_m$ (MPa)	$T_{a,max}$ (MPa)	$T_m$ (MPa)	$\delta$ (°)	$F$	$N_f$ (cycles)
S13_VA	1000RD	219.0	0.0	0.0	0.0	–	–	391,420
S17_VA	1000RD	219.0	0.0	0.0	0.0	–	–	339,763
S4_VA	1000RD	279.8	0.0	0.0	0.0	–	–	170,155
S6_VA	1000RD	279.8	0.0	0.0	0.0	–	–	182,155
S7_VA	1000RD	389.3	0.0	0.0	0.0	–	–	66,703
S9_VA	1000RD	389.3	0.0	0.0	0.0	–	–	61,594
S2_VA	1000RD	520.1	0.0	0.0	0.0	–	–	20,975
S3_VA	1000RD	520.1	0.0	0.0	0.0	–	–	21,568
S26_VA	2500L	228.1	0.0	0.0	0.0	–	–	242,271
S5_VA	2500L	228.1	0.0	0.0	0.0	–	–	272,374
S22_VA	2500L	288.9	0.0	0.0	0.0	–	–	113,624
S27_VA	2500L	288.9	0.0	0.0	0.0	–	–	112,124
S23_VA	2500L	380.2	0.0	0.0	0.0	–	–	50,089
BS_1	50BSP	136.9	0.0	136.9	0.0	0	1	207,026
BS_2	50BSP	136.9	0.0	271.0	0.0	0	1	24,348
BS_2b	50BSP	136.9	0.0	278.2	0.0	0	1	23,581
BS_3	50BSP	136.9	0.0	182.5	0.0	0	1	148,732
BS_4	50BSP	0.0	0.0	388.9	0.0	–	–	2715
BS_4b	50BSP	0.0	0.0	299.2	0.0	–	–	16,679
BS_5	50BSP	0.0	0.0	209.4	0.0	–	–	377,053
BS_6	50BSP	0.0	0.0	269.3	0.0	–	–	32,100
BS_7	50BSP	136.9	0.0	179.5	0.0	90	1	81,631
BS_8	50BSP	136.9	0.0	271.0	0.0	90	1	14,269
BS_9	50BSP	136.9	0.0	136.9	0.0	90	1	151,007
BS_10	50BSP	114.1	22.8	209.4	41.9	90	1	59,622
BS_11	50BSP	114.1	22.8	269.3	53.9	90	1	11,850
BS_12	50BSP	114.1	22.8	119.7	23.9	90	1	272,152
BS_13	50BSP	114.1	22.8	209.4	41.9	0	1	131,475
BS_14	50BSP	114.1	22.8	269.3	53.9	0	1	18,045
BS_15	50BSP	114.1	22.8	149.6	29.9	0	1	327,657
BS_16	50BSP	136.9	0.0	239.3	0.0	0	2	15,376
BS_17	50BSP	136.9	0.0	149.6	0.0	0	2	76,958
BS_18	50BSP	136.9	0.0	125.7	0.0	0	2	104,950
BS_19	50BSP	136.9	0.0	239.3	0.0	0	0.5	14,885
BS_20	50BSP	136.9	0.0	149.6	0.0	0	0.5	182,882
BS_21	50BSP	136.9	0.0	125.7	0.0	0	0.5	123,167
BS_22	50BSP	95.0	22.8	249.3	59.8	90	2	16,078
BS_23	50BSP	95.0	22.8	189.5	45.5	90	2	39,479
BS_24	50BSP	95.0	22.8	159.6	38.3	90	2	58,275
BS_25	50BSP	95.0	22.8	249.3	59.8	90	0.5	24,417
BS_26	50BSP	95.0	22.8	189.5	45.5	90	0.5	74,570
BS_27	50BSP	95.0	22.8	159.6	38.3	90	0.5	146,608

mechanisms resulting in breakage under VA biaxial fatigue loading. The failure matrix reported in Fig. 5 summarises the observed fracture surfaces that are classified in terms of both sharpness of the tested notch and complexity of the applied VA loading path. For any loading/geometrical configuration, the first and the second picture show a failure in the low- ( $N_f \cong 10^4$  cycles to failure) and in the medium-cycle fatigue regime ( $N_f \cong 10^5$ – $3 \times 10^5$  cycles to failure), respectively.

As to the failure surfaces reported in the above figure, the main features of the observed cracking processes can schematically be summarised as follows:

- **Mechanism A: crack initiation.** Under VA biaxial fatigue loading, cracks always initiated, at the notch root, on those material planes of maximum shear stress amplitude that were most closely aligned to the net cross-sectional area (Stage I). At a macroscopic level, fatigue cracks were seen to initiate at the notch root in all the tested samples, resulting in circumferential cracks radially propagating inward to the centre of the net cross sectional area.
- **Mechanism B: crack propagation.** After exhausting the initial Stage I growth, fatigue cracks kept propagating by orienting themselves in order to experience the maximum Mode I loading (Stage II). Under VA biaxial fatigue loading, this resulted in the tendency of forming conventional factory roof failure surfaces.

- **Mechanism C: shear stress rubbing phenomenon.** Since the surfaces on which the crack propagation phenomenon took place were almost coincident with the net cross-sectional areas of the tested notched samples, the nominal cyclic torque was seen to result in a rubbing effect that wore, by somehow smoothening, the two material faces of the cracks. According to the above mechanism, in many different cases the resulting fracture surfaces were also characterised by a series of concentric circular marks.

In order to understand the role played by the above three cracking mechanisms, attention can initially be focused on the results generated by testing, under fully-reversed VA torsional loading, the V-notched samples having root radius,  $r_n$ , equal to 0.225 mm. In the above specimens initiation and initial growth were seen to always occur at the notch root on the material plane perpendicular to the specimen axis (Stage I). After reaching a certain length depending on the magnitude of the applied VA torsional loading, the branching phenomenon occurred, resulting in a Stage II propagation which was governed by the maximum normal stress. Under the most damaging VA torsional load spectrum (specimen BS\_4 in Fig. 5), the preferential Stage II planes were at 45° to the specimen axis, even though the large amount of relative rotation between the two faces of the crack pushed up the material, resulting in almost vertical crests. In other words, due to the combined effect

**Table 3**

Summary of the experimental results generated by testing the notched specimens with root radius equal to 1.2 mm under VA fatigue loading.

Code	Spectrum	$\Sigma_{a,max}$ (MPa)	$\Sigma_m$ (MPa)	$T_{a,max}$ (MPa)	$T_m$ (MPa)	$\delta$ (°)	$F$	$N_f$ (cycles)
I1_VA	1000RD	520.4	0.0	0.0	0.0	–	–	37,568
I4_VA	1000RD	520.4	0.0	0.0	0.0	–	–	34,044
I2_VA	1000RD	432.4	0.0	0.0	0.0	–	–	84,463
I5_VA	1000RD	432.4	0.0	0.0	0.0	–	–	83,663
I3_VA	1000RD	344.5	0.0	0.0	0.0	–	–	170,581
I6_VA	1000RD	344.5	0.0	0.0	0.0	–	–	253,927
I10_VA	1000RD	300.5	0.0	0.0	0.0	–	–	715,859
I14_VA	1000RD	300.5	0.0	0.0	0.0	–	–	588,009
I17_VA	2500L	469.1	0.0	0.0	0.0	–	–	32,624
I20_VA	2500L	395.8	0.0	0.0	0.0	–	–	99,124
I21_VA	2500L	395.8	0.0	0.0	0.0	–	–	72,874
I18_VA	2500L	337.1	0.0	0.0	0.0	–	–	190,874
I19_VA	2500L	337.1	0.0	0.0	0.0	–	–	178,741
BI_1	50BSP	0.0	0.0	327.0	0.0	–	–	17,459
BI_2	50BSP	0.0	0.0	308.1	0.0	–	–	36,957
BI_3	50BSP	0.0	0.0	282.9	0.0	–	–	72,587
BI_4	50BSP	0.0	0.0	257.8	0.0	–	–	143,825
BI_5	50BSP	141.5	0.0	289.2	0.0	0	1	30,942
BI_6	50BSP	141.5	0.0	232.6	0.0	0	1	102,168
BI_7	50BSP	141.5	0.0	201.2	0.0	0	1	147,795
BI_8	50BSP	141.5	0.0	264.1	0.0	90	1	60,320
BI_9	50BSP	141.5	0.0	201.2	0.0	90	1	190,554
BI_29	50BSP	141.5	0.0	232.6	0.0	90	1	68,269
BI_11	50BSP	117.9	23.6	282.9	56.6	90	1	25,459
BI_12	50BSP	117.9	23.6	220.1	44.0	90	1	149,867
BI_13	50BSP	117.9	23.6	251.5	50.3	90	1	85,782
BI_14	50BSP	117.9	23.6	282.9	56.6	0	1	54,532
BI_15	50BSP	117.9	23.6	238.9	47.8	0	1	114,205
BI_16	50BSP	117.9	23.6	257.8	51.6	0	1	65,736
BI_17	50BSP	141.5	0.0	276.7	0.0	0	2	16,518
BI_18	50BSP	141.5	0.0	207.5	0.0	0	2	100,826
BI_19	50BSP	141.5	0.0	238.9	0.0	0	2	45,386
BI_20	50BSP	141.5	0.0	276.7	0.0	0	0.5	27,487
BI_21	50BSP	141.5	0.0	207.5	0.0	0	0.5	49,309
BI_22	50BSP	141.5	0.0	176.1	0.0	0	0.5	383,726
BI_23	50BSP	117.9	23.6	282.9	56.6	90	2	18,797
BI_24	50BSP	117.9	23.6	220.1	44.0	90	2	80,276
BI_25	50BSP	117.9	23.6	188.6	37.7	90	2	67,764
BI_26	50BSP	117.9	23.6	282.9	56.6	90	0.5	10,341
BI_27	50BSP	117.9	23.6	220.1	44.0	90	0.5	107,965
BI_28	50BSP	117.9	23.6	188.6	37.7	90	0.5	168,106

of a torsional loading of large magnitude and a severe stress concentration phenomenon, the Mode I cracks grew very rapidly making it hard for shear stress rubbing phenomenon to take place. Therefore, the resulting factory roof surface was just partially deformed by the interaction, occurring during the twisting motion of the cracked material, between the two faces of the crack. On the contrary, as the maximum amplitude of the torsional load spectrum decreased, the shear stress rubbing mechanism was seen to become more and more predominant, resulting in smoother failure surfaces (sample BS\_5 in Fig. 5).

A mechanism similar to the one described above occurred also in the other notched geometries tested under VA torsion, the only difference being that the effect of the rubbing mechanism was seen to increase with the decreasing of the effect, on the crack growth rate, of the stress gradient's severity.

Under in-phase biaxial VA loading instead, the shear stress governed initiation phenomenon was always followed by a Stage II propagation, resulting in conventional factory roof fracture surfaces - this holding true under both zero and non-zero mean stresses (see, for instance, surfaces BS\_1 and BI\_14 in Fig. 5). Similar to the torsional case, also under in-phase VA biaxial loading the rubbing effect tended to increase as the sharpness of the notch was reduced: the crack growth rate decreased as the severity of the stress gradient decreased, allowing the asperities resulting from the Mode I propagation to be rubbed off, either partially or completely, by the relative twisting motion of the two surfaces of the cracks (see, for instance, samples BB\_5 and BB\_14 in Fig. 5).

In order to deepen the investigation on the cracking behaviour under VA in-phase biaxial loading, some of the generated fracture surfaces were also analysed by using the Scanning Electron Microscope available at Trinity College – Dublin (Ireland), the taken pictures being reported in Fig. 6. In more detail, Fig. 6a shows a fracture surface where a crack initiated at the notch root, the observed material portion being characterised by a small amount of local plastic deformation.

Fig. 6b instead displays a crest of the factory roof, each side being characterised not only by a different slope, but also by a different aspect. In particular, one side of the asperity appears to be worn, with parallel marks resulting from the rubbing effect of the two twisting surfaces of the crack. The fact that the above marks, which are perpendicular to the radial direction along which the crests themselves formed, appears only on one side may be ascribed to the profile of the applied loading path (Fig. 4b): since the two applied nominal stress components were in-phase, the marks tended to form only during the tensile part of any biaxial cycle, that is, only when, the crack being open due to the applied tensile stress, the two surfaces of the crack could rotate more easily.

Turning back to the macroscopic cracking behaviour summarised in Fig. 5, it is worth observing here that both under out-of-phase synchronous VA biaxial loading and under in-phase/out-of-phase biaxial load spectra with a frequency ratio,  $F$ , different from unity the shear stress rubbing effect was seen to be predominant, always resulting in relatively smooth fracture surfaces (this holding true independently of magnitude of the mean stress

**Table 4**

Summary of the experimental results generated by testing the notched specimens with root radius equal to 3 mm under VA fatigue loading.

Code	Spectrum	$\Sigma_{a,max}$ (MPa)	$\Sigma_m$ (MPa)	$T_{a,max}$ (MPa)	$T_m$ (MPa)	$\delta$ (°)	$F$	$N_f$ (cycles)
B1_VA	1000RD	631.8	0.0	0.0	0.0	–	–	18,736
B2_VA	1000RD	631.8	0.0	0.0	0.0	–	–	15,715
B3_VA	1000RD	496.4	0.0	0.0	0.0	–	–	65,733
B7_VA	1000RD	496.4	0.0	0.0	0.0	–	–	63,450
B5_VA	1000RD	413.7	0.0	0.0	0.0	–	–	118,044
B8_VA	1000RD	413.7	0.0	0.0	0.0	–	–	138,975
B4_VA	1000RD	361.0	0.0	0.0	0.0	–	–	274,715
B6_VA	1000RD	361.0	0.0	0.0	0.0	–	–	300,763
B20_VA	2500L	556.6	0.0	0.0	0.0	–	–	22,498
B17_VA	2500L	481.4	0.0	0.0	0.0	–	–	61,874
B19_VA	2500L	481.4	0.0	0.0	0.0	–	–	70,624
B18_VA	2500L	421.2	0.0	0.0	0.0	–	–	88,874
B21_VA	2500L	421.2	0.0	0.0	0.0	–	–	133,874
BB_1	50BSP	0.0	0.0	364.7	0.0	–	–	12,831
BB_2	50BSP	0.0	0.0	314.4	0.0	–	–	30,107
BB_3	50BSP	0.0	0.0	295.5	0.0	–	–	84,635
BB_4	50BSP	0.0	0.0	282.9	0.0	–	–	99,207
BB_5	50BSP	141.5	0.0	327.0	0.0	0	1	17,161
BB_6	50BSP	141.5	0.0	264.1	0.0	0	1	94,483
BB_7	50BSP	141.5	0.0	245.2	0.0	0	1	98,695
BB_8	50BSP	141.5	0.0	314.4	0.0	90	1	16,337
BB_9	50BSP	141.5	0.0	251.5	0.0	90	1	136,146
BB_10	50BSP	141.5	0.0	220.1	0.0	90	1	164,490
BB_11	50BSP	117.9	23.6	314.4	62.9	90	1	10,391
BB_12	50BSP	117.9	23.6	257.8	51.6	90	1	92,073
BB_13	50BSP	117.9	23.6	226.4	45.3	90	1	344,115
BB_14	50BSP	117.9	23.6	327.0	65.4	0	1	12,502
BB_15	50BSP	117.9	23.6	282.9	56.6	0	1	49,830
BB_16	50BSP	117.9	23.6	251.5	50.3	0	1	115,047
BB_17	50BSP	141.5	0.0	295.5	0.0	0	2	28,437
BB_18	50BSP	141.5	0.0	251.5	0.0	0	2	101,333
BB_19	50BSP	141.5	0.0	220.1	0.0	0	2	206,916
BB_20	50BSP	141.5	0.0	295.5	0.0	0	0.5	20,762
BB_21	50BSP	141.5	0.0	251.5	0.0	0	0.5	80,840
BB_22	50BSP	141.5	0.0	220.1	0.0	0	0.5	128,514
BB_23	50BSP	117.9	23.6	308.1	61.6	90	2	18,042
BB_24	50BSP	117.9	23.6	264.1	52.8	90	2	38,975
BB_25	50BSP	117.9	23.6	238.9	47.8	90	2	106,213
BB_26	50BSP	117.9	23.6	308.1	61.6	90	0.5	23,912
BB_27	50BSP	117.9	23.6	264.1	52.8	90	0.5	62,360
BB_28	50BSP	117.9	23.6	238.9	47.8	90	0.5	135,815

and sharpness of the tested notch). As to the above situation, it is initially interesting to notice that, as shown in Fig. 4a, under biaxial loading at different frequencies the situation was, in terms of profile of the single cycle loading path, always similar to the one obtained under out-of-phase synchronous VA biaxial loading. Accordingly, during testing, when the applied nominal torque reached its relative maximum value, the corresponding axial nominal stress was always equal to zero. In this situation, the rubbing effect due to torque was seen to prevail over the cracking mechanism leading to the formation of factory roof crests, resulting, as said above, in relatively smooth fracture surfaces (see Fig. 5).

Finally, to clearly show the morphological features of the cracked material resulting from the shear stress rubbing mechanism in the presence of reduced stress concentration phenomena, Fig. 6c and d shows two different portions of the fracture surface in bluntly notched specimen BB\_3. According to the above pictures, the morphology of the corrugate surface displayed by the bluntest samples may be related to the fact that growing cracks always tried to form factory roof features (by twisting around to 45-degrees), these features continually being deformed and pushed over. The fact that the crack initiation phenomenon could take place also in the material volume is supported by the large amount of plastic deformation observed in the internal regions of the fracture surfaces. Subsequently, these cracks grew, presumably on the planes of maximum normal stress, until a conventional coalescence phenomenon took place. Thus these new long cracks standing on dif-

ferent planes were subsequently deformed by the torsional loading, creating almost vertical cracks, grouped in contiguous sheets (Fig. 6c and d).

## 7. Validation by experimental results

The experimental results (see Tables 2–4) generated by testing the V-notched cylindrical samples of carbon steel C40 (Fig. 3a) under the three investigated load spectra (Fig. 4) were used to systematically check the accuracy of our critical distance/plane approach in estimating lifetime under VA fatigue loading.

The necessary linear-elastic stress fields in the vicinity of the notch tip of the tested specimens were determined, through commercial software ANSYS®, by solving refined FE models, the density of the mapped mesh being gradually refined until convergence has occurred.

The unnotched results obtained under fully-reversed CA axial and torsional loading (see Fig. 3b and Table 1) were initially used to calibrate the constants in the MWCM's governing equations, Eqs (2)–(5), as well as to calculate the limit value of ratio  $\rho_{eff}$ , Eq. (6), i.e.,  $\rho_{lim} = 1.358$ .

The CA fully-reversed unnotched fatigue curve together with the CA fatigue curve determined by testing V-notched samples with root radius equal to 0.225 mm (Table 1) were subsequently used, according to the standard procedure we have proposed [25,38,39], to calibrate the constants in the  $L_M$  vs.  $N_f$  relationship, by obtaining [41]:



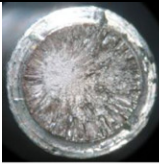
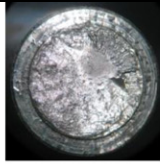
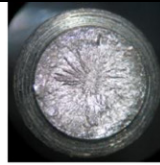
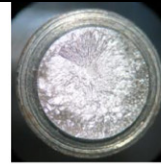
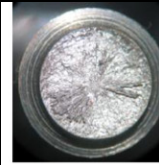
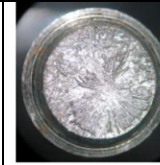


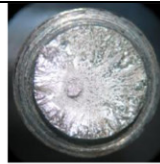

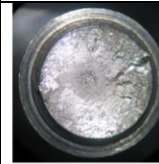
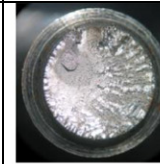
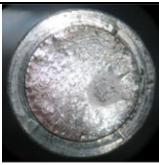

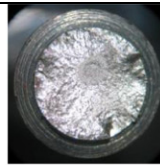
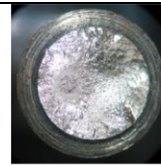
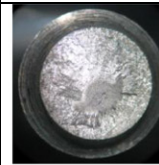
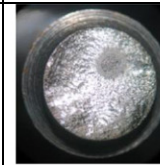



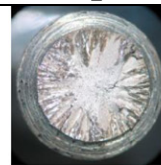
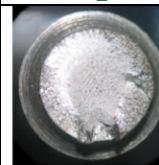
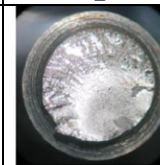
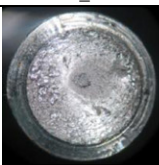
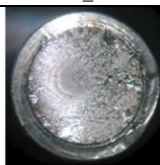
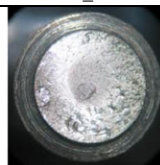
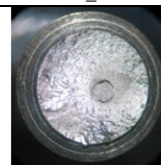
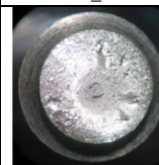
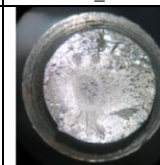


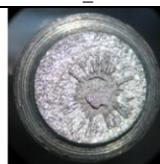
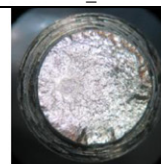
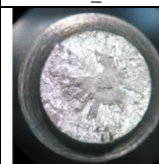
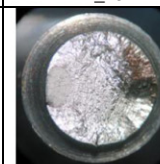

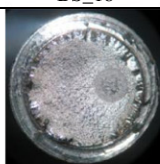
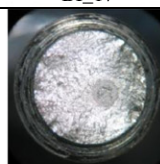
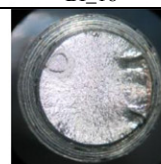
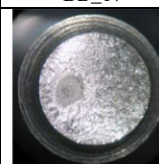
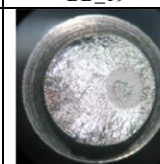
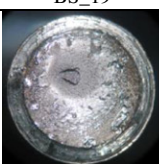

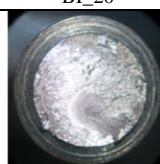
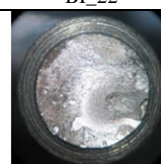
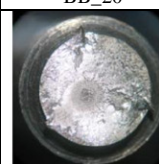
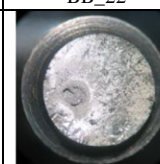


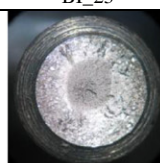
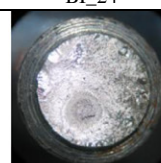
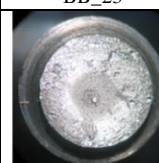
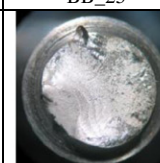
	$r_n=0.225$ mm		$r_n=1.2$ mm		$r_n=3$ mm	
50BSP T ZMS	 BS_4	 BS_5	 BI_1	 BI_4	 BB_1	 BB_4
50BSP Bi ZMS IPh F=1	 BS_2b	 BS_1	 BI_5	 BI_7	 BB_5	 BB_7
50BSP Bi ZMS OoPh F=1	 BS_8	 BS_9	 BI_8	 BI_9	 BB_8	 BB_10
50BSP Bi N-ZMS IPh F=1	 BS_14	 BS_15	 BI_14	 BI_15	 BB_14	 BB_16
50BSP Bi N-ZMS OoPh F=1	 BS_11	 BS_10	 BI_11	 BI_12	 BB_11	 BB_13
50BSP Bi ZMS IPh F=2	 BS_16	 BS_18	 BI_17	 BI_18	 BB_17	 BB_19
50BSP Bi ZMS IPh F=0.5	 BS_19	 BS_20	 BI_20	 BI_22	 BB_20	 BB_22
50BSP Bi N-ZMS OoPh F=2	 BS_22	 BS_24	 BI_23	 BI_24	 BB_23	 BB_25
50BSP Bi N-ZMS OoPh F=0.5	 BS_25	 BS_27	 BI_26	 BI_28	 BB_26	 BB_28

Fig. 5. Matrix of the observed fracture surfaces.



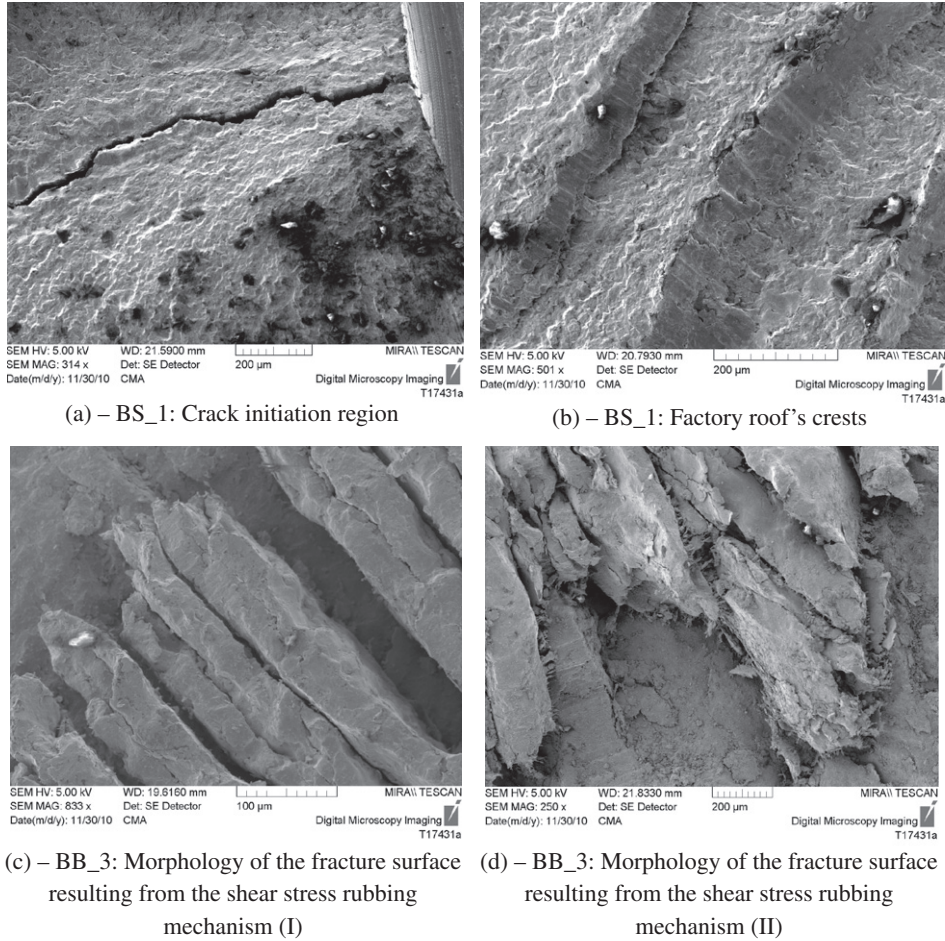


Fig. 6. Fracture surfaces investigated with a scanning electron microscope.

$$L_M(N_f) = 6.05 \cdot N_f^{-0.286} \quad (\text{mm}) \quad (28)$$

The unnotched fatigue curve generated under zero-tension by testing unnotched samples and having endurance limit,  $\sigma_{A,R=0}$ , equal to 260 MPa (Table 1) was employed instead to calculate the mean stress sensitivity index. In particular, by observing that under the above simple loading path the stress components relative to the critical plane were as follows [25]:

$$\tau_a^* = \sigma_{n,a}^* = \sigma_{n,m}^* = \frac{\sigma_{A,R=0}}{2} = 130 \text{ MPa},$$

mean stress sensitivity index  $m$  took on the following value [25,39]:

$$m = \frac{\tau_a^*}{\sigma_{n,m}^*} \left( 2 \frac{\tau_A - \tau_a^*}{2\tau_A - \sigma_A} - \frac{\sigma_{n,a}^*}{\tau_a^*} \right) = 0.19 \quad (29)$$

In order to estimate the fatigue lifetime of the tested notched samples, the procedure summarised in Fig. 2 was implemented by developing an *ad hoc* post-processor capable of solving two different multivariable optimisation problems in parallel: the first algorithm was based on the gradient ascent method and it was designed to determine the orientation of the critical plane through the direction experiencing the maximum variance of the resolved shear stress [47]; the second algorithm, taking full advantage of the simple bisection method, was instead used to determine critical distance  $L_M$ , Eq. (23), from the equivalent number of cycles to failure,  $N_{f,eq}$ , calculated according to definition (22).

The overall accuracy of our method in estimating the fatigue lifetime of the tested V-notched samples is summarised in the experimental,  $N_f$ , vs. estimated,  $N_{f,e}$ , number of cycles to failure

diagrams reported in Fig. 7, the knee points being taken, as recommended by Sonsino [49], at  $N_{kp} = 2 \times 10^6$  cycles to failure. In more detail, the above charts were built by initially assuming, as suggested by Palmgren [56] and Miner [57], that the critical value of the damage sum,  $D_{cr}(\bar{\rho}_{eff})$ , was constant and invariably equal to unity. The above diagrams make it evident that the use of our method resulted in estimates characterised by a slight degree of conservatism, but all falling within the widest scatter band between the two associated with the CA unnotched experimental results used to calibrate the constants in the MWCM's governing equation. Such a high level of accuracy was obtained independently of sharpness of the tested notch as well as of complexity and profile of the applied VA load history. It is evident that the above results are definitely satisfactory, since we cannot ask a predictive method to be, from a statistical point of view, more accurate than the experimental information used to calibrate the approach itself.

Another important outcome which deserves to be highlighted here is that our critical distance/plane approach was seen to be highly accurate in estimating also the results generated under VA uniaxial nominal loading: this confirms that the design strategy proposed in the present paper is capable of correctly taking into account the degree of multiaxiality of the post-processed stress field also when the source of such a multiaxiality is a geometrical feature and not the complexity of the applied VA load history.

Turning back to the overall accuracy shown by the charts of Fig. 7, by sharply observing the distribution of the estimates it is straightforward to come to the conclusion that the tested carbon steel had an actual value of the critical damage sum that was not



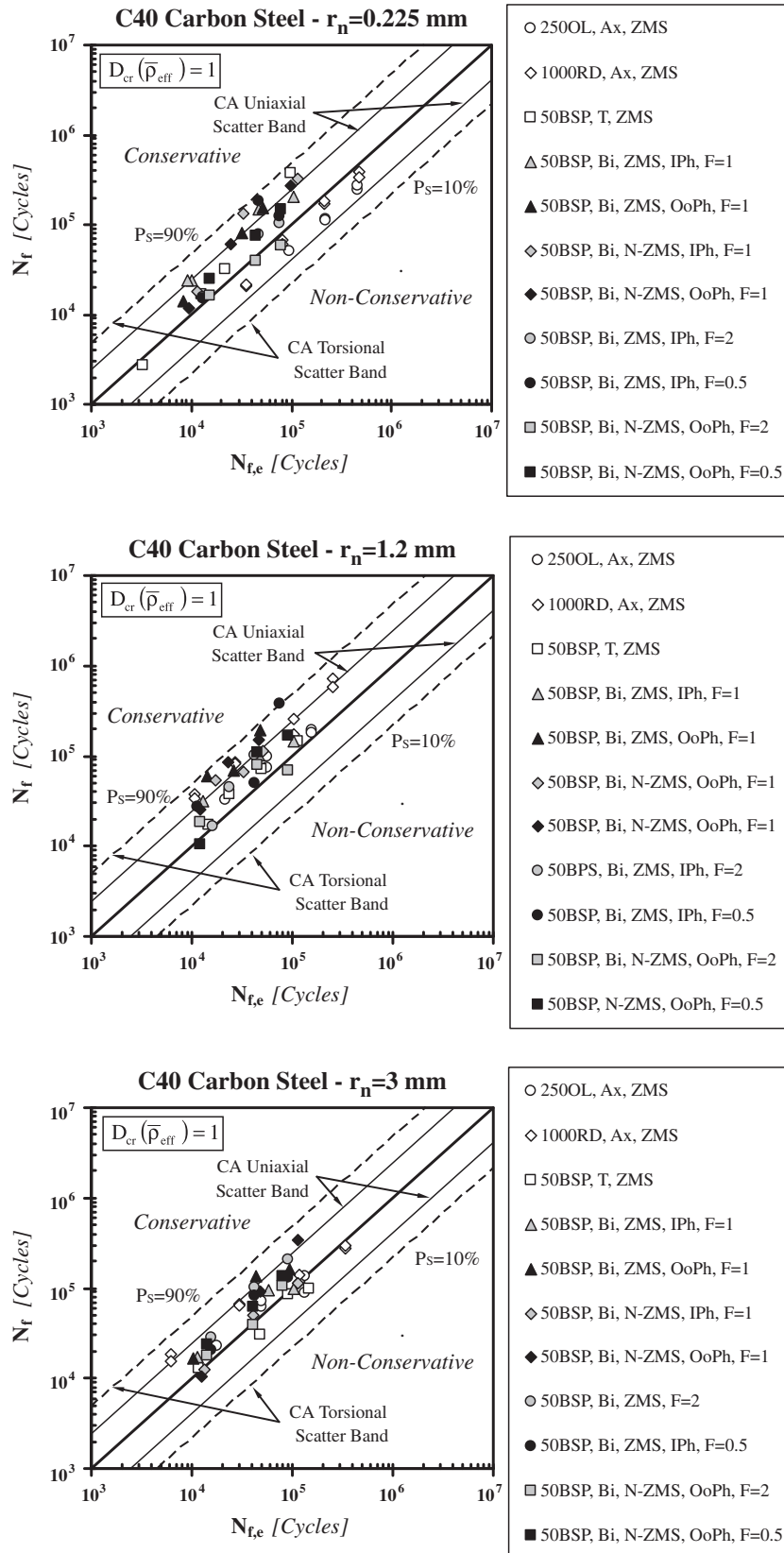


Fig. 7. Accuracy of the proposed method in estimating the lifetime of the notched samples tested under uniaxial and biaxial VA fatigue loading by taking  $D_{cr}$  equal to unity.

only close to unity, but also quite independent on the degree of multiaxiality of the applied VA loading path. The above remarks are fully confirmed by the chart of Fig. 8a which plots, for any

generated results, the experimental value of the critical damage sum against the effective value of the critical plane stress ratio,  $\bar{\rho}_{eff}$ : according to the above diagram the distribution of the exper-

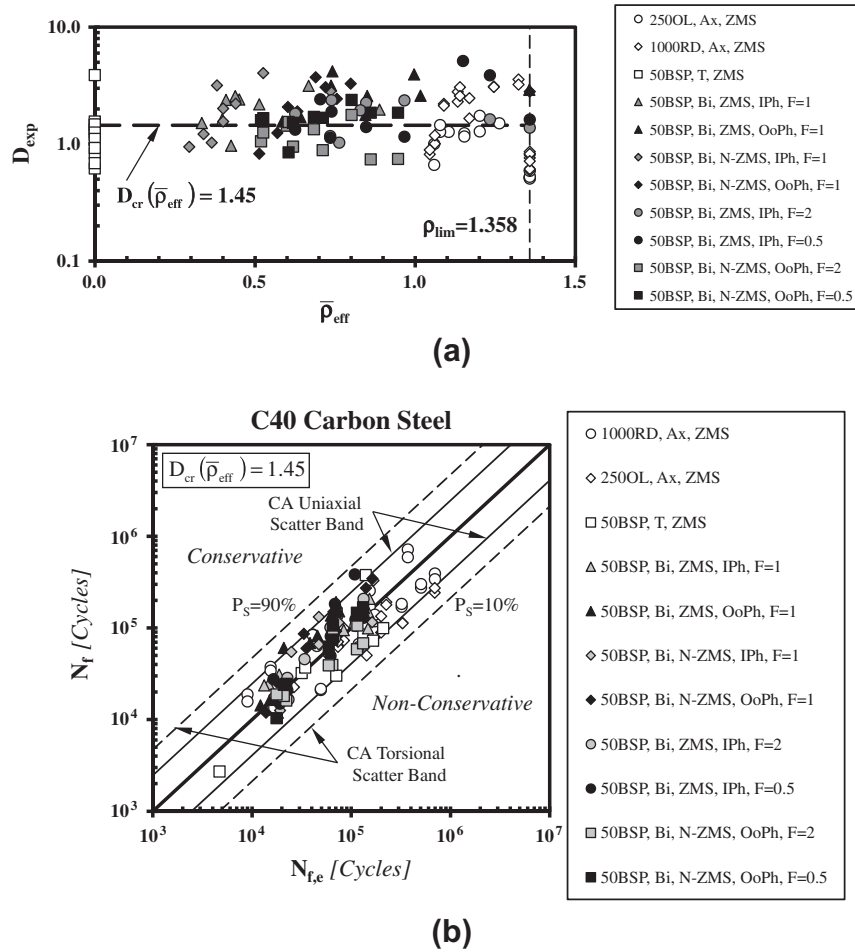


Fig. 8. Experimental value of the damage sum,  $D_{exp}$ , against ratio  $\bar{\rho}_{eff}$  (a) and accuracy of the proposed method in estimating the lifetime of the notched samples tested under uniaxial and biaxial VA fatigue loading by taking  $D_{cr}$  equal to 1.45 (b).

Table 5

Fatigue properties of the materials used to check the accuracy of the proposed approach through experimental data taken from the literature.

Material	Ref.	R	k	$\sigma_A^a$ (MPa)	$\tau_A^a$ (MPa)	$T_\sigma$	$T_\tau$	$\rho_{lim}$	m	B	A (mm/cycles) <sup>B</sup>	$N_{kp}$ (cycles)
SAE 1045	[23]	-1	9.0	195.8	-	1.151	-	3.24	1	-0.151	25.8	$2 \times 10^6$ [49]
		-1	10.2	-	115.8	-	1.148	-	-	-	-	-
S460N	[58,59]	-1	10.3	228.3	-	1.151	-	1.99	1	-0.093	4.8	$2 \times 10^6$ [49]
		-1	13.4	-	152.5	-	1.049	-	-	-	-	-
Fe 460 (welded)	[54,60]	-1	8.3	217.3	-	1.489	-	3.15	1	-0.386	89.4	$10^8$ [61,62]
		-1	9.4	-	129.15	-	1.344	-	-	-	-	-

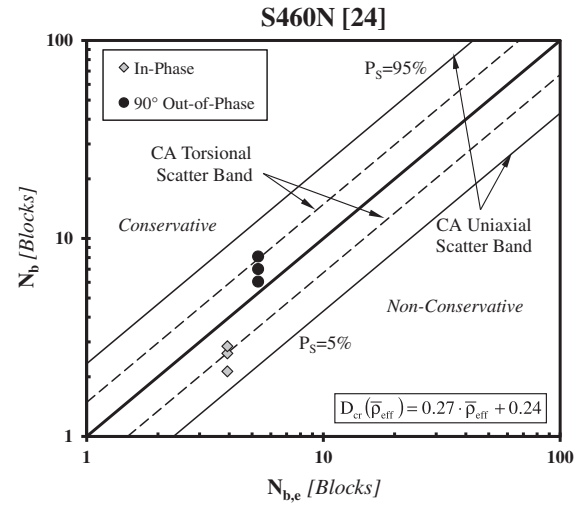
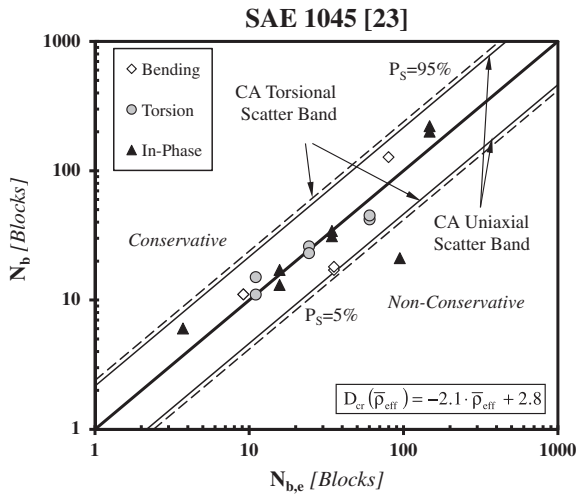
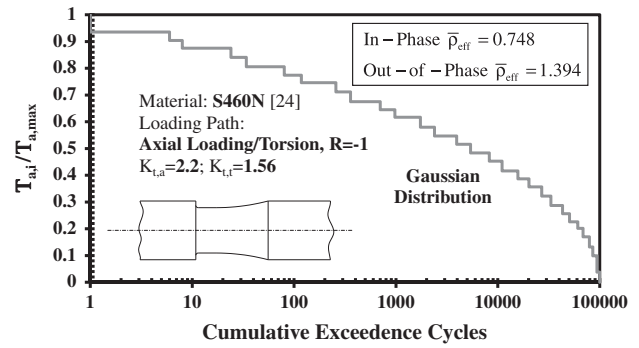
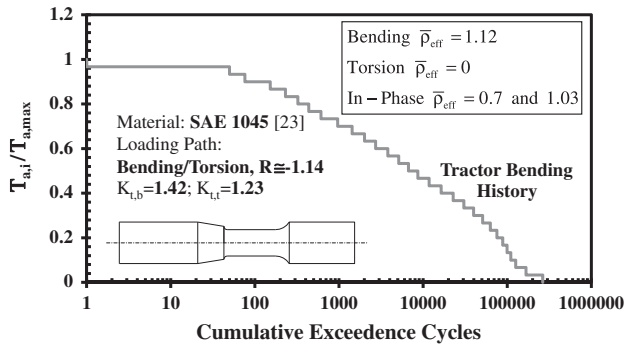
<sup>a</sup> Reference stress amplitude extrapolated at  $2 \times 10^6$  cycles to failure.

imental point, which shows the usual scattering characterising fatigue results, follows an horizontal straight trend line, confirming that, for the tested steel,  $D_{cr}(\bar{\rho}_{eff})$  could be assumed to be independent from  $\bar{\rho}_{eff}$  with little loss of accuracy. According to the above consideration, as an example the error diagram reported in Fig. 8b summarises the accuracy of our approach in estimating all the results we generated by taking the critical value of the damage sum equal to 1.45, that is, equal to the value calculated by averaging the results generated under uniaxial and torsional VA loading: a value of  $D_{cr}(\bar{\rho}_{eff})$  equal to 1.45 clearly allowed the level of conservatism of the estimates to be reduced, by resulting in highly accurate predictions (Fig. 8b). To conclude, it is worth observing that the critical value of the damage sum calculated by averaging all the experimental results reported in the chart of Fig. 8a was seen to be equal to 1.77, that is, within the

experimental range 0.02–5 that is commonly observed in situations of practical interest [51].

In light of the encouraging accuracy obtained by reanalysing the experimental results we generated, the accuracy of our critical distance/plane approach was subsequently attempted to be checked through several data sets taken from the literature, where Table 5 summarises the fatigue properties of the investigated materials.

In more detail, initially we considered the results generated by testing notched samples of SAE 1045 under load history “Ag Tractor Bending”, that is, a VA in-phase bending and torsion load history gathered from an instrumented drive axle of an agriculture tractor and summarised through a Markovian matrix [23,63]. The notched samples investigated in the SAE Biaxial Program were conventional cylindrical shafts with fillet (Fig. 9), where the notch root radius of 5 mm resulted in a stress concentration factor of 1.42



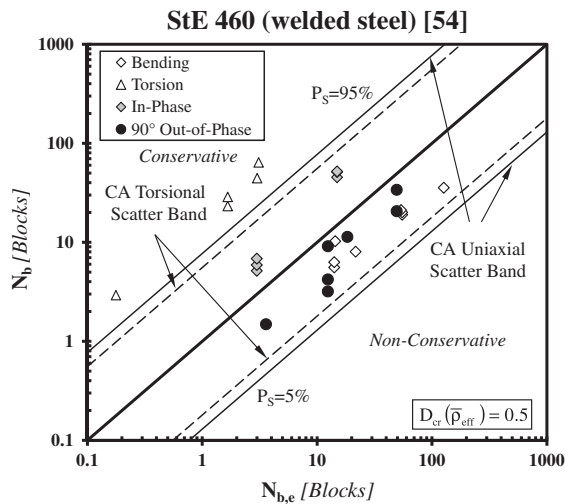
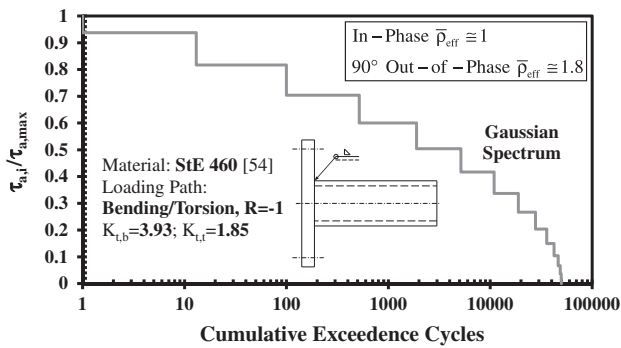
**Fig. 9.** Accuracy of the proposed method in estimating the lifetime of the notched samples with fillet of SAE 1045 [23,61] tested under bending and torsion VA fatigue loading.

**Fig. 10.** Accuracy of the proposed method in estimating the lifetime of the notched samples with fillet of S460N [24] tested under axial loading and torsion VA fatigue loading.

under bending and of 1.23 under torsion. The experimental,  $N_b$ , vs. estimated  $N_{b,e}$ , blocks to failure diagram reported in Fig. 9 fully confirms that our approach was highly accurate also in estimating such classical results. As to the above accuracy level, it is worth observing here that the adopted  $D_{cr}(\bar{\rho}_{eff})$  was calibrated by using the results generated under both uniaxial and torsional VA loading, since the critical value under simple bending was seen to be much lower than the corresponding value under torsion. This should further confirm what was already observed by Sonsino and Kueppers [54]: given the material and the geometrical feature, the critical value of the damage sum can vary as the degree of multiaxiality and non-proportionality of the applied load history varies, so that, such a tricky aspect of the problem must always be addressed very carefully when designing real components against VA fatigue.

Subsequently, we considered the results generated by Vormwald and co-workers [24] by testing cylindrical samples with fillet of steel S460N under the in-phase and 90° out-of-phase biaxial load spectrum reported in Fig. 10. As to the calibration constants characterising the above material and listed in Table 5, it has to be pointed out that the uniaxial and torsional unnotched fatigue curves were directly estimated from the corresponding strain-controlled results. Further, due to a lack of suitable data, the  $L_M$  vs.  $N_f$  relationship was calibrated through the notch results generated under CA in-phase and 90° out-of-phase biaxial loading, i.e., by directly extending the use of the procedure proposed in Ref. [39] to situations involving multiaxial fatigue loading. Finally, function  $D_{cr}(\bar{\rho}_{eff})$  was roughly calibrated by using a conventional best-fit procedure. In spite of the above simplifications, the accuracy shown by the error diagram reported in Fig. 10 is satisfactory also for the notched samples of S460N.

Subsequently, our attention was focused on the data generated by Sonsino and Kueppers [54] by testing tube-to-plate steel welded joints under Gaussian spectra having sequence length,  $n_{tot}$ , equal to  $5 \times 10^4$  cycles (Fig. 11). In particular, since the average value of the weld toe radius was directly reported in Ref. [54], i.e.,  $r_n = 0.45$  mm, the above samples were treated as notched components. In other words, such results were used to check the accuracy of the approach proposed in the present paper by explicitly modelling the weld toe radius, and not, as done elsewhere [64,65], by taking it invariably equal to zero. The constants in the MWCM's governing equations were calculated by using the CA fully-reversed bending and torsion curves generated by testing tube-to-tube ground butt welded samples of Ste 460 [60]. The  $L_M$  vs.  $N_f$  relationship was instead calibrated by using the CA fully-reversed bending curve experimentally determined through the tube-to-tube ground butt welded joints [60] as well as the CA fully-reversed curve generated by testing under bending the tube-to-plate welded samples [54] (Table 5). Finally, the estimates summarised in the error diagram of Fig. 11 were calculated by taking, as recommended by the IIW [61], the critical value of the damage sum,  $D_{cr}(\bar{\rho}_{eff})$ , constant and equal to 0.5. The above chart shows that the predictions made for the results generated under VA torsion were characterised by a slight degree of conservatism, whereas, under the other VA loading paths, estimates are seen to fall within the CA uniaxial scatter band. As to the above chart, it is worth observing that any series of data is aligned to the diagram bisector, confirming that the use of our approach results in accurate estimates, provided that function  $D_{cr}(\bar{\rho}_{eff})$  is calibrated accurately. At the same time, Fig. 11 makes it evident that the overall accuracy of the predictions varies as  $\bar{\rho}_{eff}$  changes: this fact is not surprising at all, since, as observed by



**Fig. 11.** Accuracy of the proposed method in estimating the lifetime of the notched samples with fillet of Ste 460 (welded steel) [54] tested under bending and torsion VA fatigue loading.

Sonsino and Kueppers themselves [54], in the above welded samples the value of the critical damage sum was seen to vary as the degree of multiaxiality and non-proportionality of the applied VA load history changed.

It is possible to conclude by observing that the validation exercise summarised in the present section seems to strongly support the idea that the proposed approach is highly accurate in estimating fatigue damage in notched components locally damage by VA multiaxial stress fields. At the same time, it has to be said that, as already highlighted by Sonsino [51], the most critical aspect in designing real components against VA fatigue is the correct evaluation of the critical value of the damage sum, the experimental approach being still the most reliable one. Accordingly, even though a big effort has already been made by the scientific community to devise specific theories suitable for more accurately estimating cumulative fatigue damage under VA fatigue loading [66], more work needs to be done in this area in order to formalise accurate theories capable of accurately estimating the critical value of the damage sum *a priori*. To conclude, it has to be admitted that the above task is not simple at all, since it is seen from the experiments that, given the material, the critical value of the damage sum varies as both the profile of the assessed load spectrum, the load ratio, the sharpness of the notch and the degree of multiaxiality and non-proportionality of the applied loading vary [46,51,54].

## 8. Conclusions

- (1) The high level of accuracy shown by the critical distance/ plane method formalised in the present paper is definitely promising: thanks to its peculiar features, our approach

can be used to design real notched components against VA uniaxial/multiaxial fatigue loading by directly post-processing the relevant stress fields determined through conventional linear-elastic FE models.

- (2) By assuming that the crack initiation phenomenon is always shear stress governed, a high level of accuracy in estimating fatigue lifetime under VA multiaxial fatigue loading was always obtained even though the cracking behaviour displayed by the tested notched samples was rather complex.
- (3) To properly design notched components against VA uniaxial/multiaxial fatigue by taking full advantage of the method formalised and validated in the present paper, the most tricky issue to be addressed in situations of practical interest is the correct definition of the critical value of damage sum.
- (4) Since the examination of the state of the art makes it clear that none of the methods devised so far allows the critical value of the damage sum to accurately be estimated without running appropriate experiments, it is evident that more work needs to be done by the scientific community to devise a sound theory allowing such a basic problem to be addressed efficiently.

## References

- [1] Łagoda T, Macha E. Estimated and experimental fatigue lives of 30CrNiMo8 steel under in- and out-of-phase combined bending and torsion with variable amplitude. *Fatigue Fract Eng Mater Struct* 1994;11:1307–18.
- [2] Morel F. A critical plane approach for life prediction of high cycle fatigue under multiaxial variable amplitude loading. *Int J Fatigue* 2000;22:101–19.
- [3] Carpinteri A, Spagnoli A, Vantadori S. A multiaxial fatigue criterion for random loading. *Fatigue Fract Engng Mater Struct* 2003;26:515–22.
- [4] Łagoda T, Ogonowski P. Criteria of multiaxial random fatigue based on stress, strain and energy parameters of damage in the critical plane. *Mat-wiss u Werkstofftech* 2005;36:429–37.
- [5] Marciniak Z, Rozumek D, Macha E. Fatigue lives of 18G2A and 10HNAP steels under variable amplitude and random non-proportional bending with torsion. *Int J Fatigue* 2008;30:800–13.
- [6] Langlais TE, Vogel JH, Chase TR. Multiaxial cycle counting for critical plane methods. *Int J Fatigue* 2003;25:641–7.
- [7] Wang CH, Brown MW. Life prediction techniques for variable amplitude multiaxial fatigue – Part 1: Theories. *Trans ASME, J Eng Mater Technol* 1996;118:367–70.
- [8] Wang CH, Brown MW. Life prediction techniques for variable amplitude multiaxial fatigue – Part 2: Comparison with experimental results. *Trans ASME, J Eng Mater Technol* 1996;118:371–4.
- [9] Kim KS, Park JC, Lee JW. Multiaxial fatigue under variable amplitude loads. *Trans ASME, J Eng Mater Technol* 1999;121:286–93.
- [10] Kim KS, Park JC. Shear strain based multiaxial fatigue parameters applied to variable amplitude loading. *Int J Fatigue* 1999;21:475–83.
- [11] Chen X, Jin D, Kim S. A weight function-critical plane approach for low-cycle fatigue under variable amplitude multiaxial loading. *Fatigue Fract Eng Mater Struct* 2006;29:331–9.
- [12] Smith KN, Watson P, Topper TH. A stress-strain function for the fatigue of metals. *J Mater* 1970;5:767–76.
- [13] Socie DF. Fatigue damage models. *Trans ASME, J Eng Mater Technol* 1987;109:293–8.
- [14] Kandil FA, Brown MW, Miller KJ. Biaxial low-cycle fatigue fracture of 316 stainless steel at elevated temperature. *Met Soc London* 1982;280:203–10.
- [15] Wang CH, Brown MW. A path-independent parameter for fatigue under proportional and non-proportional loading. *Fatigue Fract Eng Mater Struct* 1993;16:1285–98.
- [16] Fatemi A, Socie DF. A critical plane approach to multiaxial fatigue damage including out-of-phase loading. *Fatigue Fract Eng Mater Struct* 1988;14:149–65.
- [17] Bannantine JA, Socie DF. A variable amplitude multiaxial life prediction method. In: Kussmaul K, McDiarmid D, Socie D, editors. *Fatigue under biaxial and multiaxial loading*. ESIS 10, London: Mechanical Engineering Publications; 1991. p. 35–51.
- [18] Pitoiset X, Preumont A, Kernilis A. Tools for multiaxial fatigue analysis of structures submitted to random vibrations. In: *Proceedings of european conference on spacecraft structures, materials and mechanical testing*, Braunschweig, Germany; 4–6 November 1998.
- [19] Pitoiset X, Rychlik I, Preumont A. Spectral methods to estimate local multiaxial fatigue failure for structures undergoing random vibrations. *Fatigue Fract Eng Mater Struct* 2001;24:715–27.

- [21] Łagoda T, Macha E, Nielslony A. Fatigue life calculation by means of the cycle counting and spectral methods under multiaxial random loading. *Fatigue Fract Eng Mater Struct* 2005;28:409–20.
- [22] Nielslony A, Macha E. Spectral method in multiaxial random fatigue. Berlin, Germany: Springer-Verlag; 2007.
- [23] Kurath P, Downing SD, Galliard DR. Summary of non-hardened notched shaft - round robin program. In: Leese GE, Socie DF, editors. Multiaxial fatigue - analysis and experiments. SAE AE-14; 1989. p. 13–32.
- [24] Hertel O, Vormwald M. Fatigue lifetime assessment of notched components under multiaxial variable amplitude loading based on a short crack growth concept. In: Carpinteri A, Pook L, Sonsino CM, editors. Proceedings of ICMFF9; 7–9 June 2010. [Parma (Italy)].
- [25] Susmel L. Multiaxial notch fatigue: from nominal to local stress-strain quantities. Cambridge (UK): Woodhead & CRC; 2009.
- [26] Taylor D. The theory of critical distances: a new perspective in fracture mechanics. Elsevier Science; 2007.
- [27] Susmel L, Lazzarin P. A Bi-parametric modified wöhler curve for high cycle multiaxial fatigue assessment. *Fatigue Fract Eng Mater Struct* 2002;25: 63–78.
- [28] Kanazawa K, Miller KJ, Brown MW. Low-cycle fatigue under out-of-phase loading conditions. *Trans ASME, J Eng Mater Technol* 1977;222–8.
- [29] Socie DF. Multiaxial fatigue damage models. *Trans ASME, J Eng Mater Technol* 1987;109:293–8.
- [30] Susmel L. Multiaxial fatigue limits and material sensitivity to non-zero mean stresses normal to the critical planes. *Fatigue Fract Eng Mater Struct* 2008;31:295–309.
- [31] Susmel L, Petrone N. Multiaxial fatigue life estimations for 6082-T6 cylindrical specimens under in-phase and out-of-phase biaxial loadings. In: Carpinteri A, de Freitas M, Spagnoli A, editors. Biaxial and multiaxial fatigue and fracture. Elsevier andESIS; 2003. p. 83–104.
- [32] Lazzarin P, Susmel L. A stress-based method to predict lifetime under multiaxial fatigue loadings. *Fatigue Fract Eng Mater Struct* 2003;26:1171–87.
- [33] Susmel L, Tovo R, Lazzarin P. The mean stress effect on the high-cycle fatigue strength from a multiaxial fatigue point of view. *Int J Fatigue* 2005;27:928–43.
- [34] Kaufman RP, Topper T. The influence of static mean stresses applied normal to the maximum shear planes in multiaxial fatigue. In: Carpinteri A, de Freitas M, Spagnoli A, editors. Biaxial and multiaxial fatigue and fracture. Elsevier andESIS; 2003. p. 123–43.
- [35] Susmel L, Taylor D. Two methods for predicting the multiaxial fatigue limits of sharp notches. *Fatigue Fract Eng Mater Struct* 2003;26:821–33.
- [36] Susmel L. A unifying approach to estimate the high-cycle fatigue strength of notched components subjected to both uniaxial and multiaxial cyclic loadings. *Fatigue Fract Eng Mater Struct* 2004;27:391–411.
- [37] Susmel L, Taylor D. A simplified approach to apply the theory of critical distances to notched components under torsional fatigue loading. *Int J Fatigue* 2006;28:417–30.
- [38] Susmel L, Taylor D. A novel formulation of the theory of critical distances to estimate lifetime of notched components in the medium-cycle fatigue regime. *Fatigue Fract Eng Mater Struct* 2007;30:567–81.
- [39] Susmel L, Taylor D. The Modified Wöhler Curve method applied along with the theory of critical distances to estimate finite life of notched components subjected to complex multiaxial loading paths. *Fatigue Fract Eng Mater Struct* 2008;31:1047–64.
- [40] Peterson RE. Stress concentration factors. New York, USA: John Wiley & Sons; 1974.
- [41] Susmel L, Taylor D. The theory of critical distances to estimate lifetime of notched components subjected to variable amplitude uniaxial fatigue loading. *Int J Fatigue* 2011;33:900–11.
- [42] Macha E. Simulation investigations of the position of fatigue fracture plane in materials with biaxial loads. *Materialwiss Werkstofftech* 1989;20(4):132–6.
- [43] Tovo R, Susmel L, Cristofori A, Benasciutti D. Le verifiche di resistenza a fatica in sollecitazioni multiassiali ad ampiezza variabile. In: Susmel L, Tovo R, Ferrara editors. Proc. of IGF Workshop on Multiaxial Fatigue, (Italy), June 5–6, 2005; 2005. p. 81–96 [ISBN 88-86281-97-8].
- [44] Susmel L, Tovo R, Benasciutti D. A novel engineering method based on the critical plane concept to estimate lifetime of weldments subjected to variable amplitude multiaxial fatigue loading. *Fatigue Fract Eng Mater Struct* 2009;32:441–59.
- [45] Kihl DP, Sarkani S, Beach JE. Stochastic fatigue damage accumulation under broadband loadings. *Int J Fatigue* 1995;17:321–9.
- [46] Susmel L, Tovo R. Estimating fatigue damage under variable amplitude multiaxial fatigue loading. *Fatigue Fract Eng Mater Struct* 2011;34:1053–77.
- [47] Susmel L. A simple and efficient numerical algorithm to determine the orientation of the critical plane in multiaxial fatigue problems. *Int J Fatigue* 2010;32:1875–83.
- [48] Haibach E. Betriebsfestigkeit—Verfahren und Daten zur Bauteilberechnung. Düsseldorf, Germany: VDI-Verlag GmbH; 1989.
- [49] Sonsino CM. Course of SN-curves especially in the high-cycle fatigue regime with regard to component design and safety. *Int J Fatigue* 2007;29:2246–58.
- [50] Matsuishi M, Endo T. Fatigue of metals subjected to varying stress. Presented to the Japan Society of Mechanical Engineers, Fukuoka, Japan; 1968.
- [51] Sonsino CM. Fatigue testing under variable amplitude loading. *Int J Fatigue* 2007;29 6:1080–9.
- [52] Anon. Eurocode No. 3. Part 1: General design rules for steel constructions. DIN-V ENV 1993-1-1/A2.
- [53] Hobbacher A. Recommendations for fatigue design of welded joints and components. IIW Document XIII-2151-07/XV-1254-07, 2007.
- [54] Sonsino CM, Kueppers M. Multiaxial fatigue of welded joints under constant and variable amplitude loadings. *Fatigue Fract Eng Mater Struct* 2001;24:309–27.
- [55] Spindel JE, Haibach E. Some considerations in the statistical determination of the shape of S-N curves. In: Little RE, Ekvall JC, editors. Statistical Analysis of Fatigue Data, ASTM STP 744; 1981. p. 89–113.
- [56] Palmgren A. Die Lebensdauer von Kugellagern. vol. 68. Verfahrenstechnik, Berlin, 1924. p. 339–41.
- [57] Miner MA. Cumulative damage in fatigue. *J Appl Mech* 1945;67:A159–64.
- [58] Hoffmeyer J, Doring R, Seeger T, Vormwald M. Deformation behaviour, short crack growth and fatigue lives under multiaxial nonproportional loading. *Int J Fatigue* 2006;28:508–20.
- [59] Jiang Y, Hertel O, Vormwald M. An experimental evaluation of three critical plane multiaxial fatigue criteria. *Int J Fatigue* 2007;29:1490–502.
- [60] Sonsino CM. Fatigue behaviour of welded components under complex elasto-plastic multiaxial deformation. LBF-Bericht Nr. 6078; 1994.
- [61] Hobbacher A. Recommendations for fatigue design of welded joints and components. IIW Document XIII-2151-07/XV-1254-07; 2007.
- [62] Susmel L, Sonsino CM, Tovo R. Accuracy of the Modified Wöhler Curve Method applied along with the  $r_{ref} = 1$  mm concept in estimating lifetime of welded joints subjected to multiaxial fatigue loading. *Int J Fatigue* 2011;33:1075–91.
- [63] Fash JW, Conle FA, Minter GL. Analysis of irregular loading histories for the SAE biaxial fatigue program. In: Leese GE, Socie DF, editors. Multiaxial fatigue - analysis and experiments. SAE AE-14; 1989. p. 33–59.
- [64] Susmel L. Modified Wöhler Curve Method, Theory of Critical Distances and EUROCODE 3: a novel engineering procedure to predict the lifetime of steel welded joints subjected to both uniaxial and multiaxial fatigue loading. *Int. J. Fatigue* 2008;30:888–907.
- [65] Susmel L. Estimating fatigue lifetime of steel weldments locally damaged by variable amplitude multiaxial stress fields. *Int J Fatigue* 2010;32:1057–80.
- [66] Fatemi A, Yang L. Cumulative fatigue damage and life prediction theories: a survey of the state of the art for homogeneous materials. *Int J Fatigue* 1998;20(1):9–34.